Carbon Dioxide and Methane Dynamics in a Peatland Headwater Stream: Origins, Processes and Implications

Pierre Taillardat, Pascal Bodmer, Charles Deblois, Alex Ponçot, Antonin Prijac, Khawla Riahi, Laure Gandois, Paul del Giorgio, Marc André Bourgault, Alain Tremblay, et al.

JGR Biogeosciences

RESEARCH ARTICLE
10.1029/2022JG006855

Carbon Dioxide and Methane Dynamics in a Peatland Headwater Stream: Origins, Processes and Implications

Pierre Taillardat[1,2], Pascal Bodmer[3], Charles P. Deblois[4], Alex Ponçot[2], Antonin Prijac[2,3], Khawla Riahi[5], Laure Gandois[6], Paul A. del Giorgio[3], Marc André Bourgault[7], Alain Tremblay[8], and Michelle Garneau[2,3]

[1]Integrated Tropical Peatland Research Programme (INTPREP), National University of Singapore, Kent Ridge, Singapore, [2]Geotop, Université du Québec à Montréal, Montréal, QC, Canada, [3]Groupe de Recherche Interuniversitaire en Limnologie (GRIL), Université du Québec à Montréal, Montréal, QC, Canada, [4]Aqua Consult, Kitchener, ON, Canada, [5]Institut National de la Recherche Scientifique, Quebec City, QC, Canada, [6]Laboratoire d'Ecologie Fonctionnelle et Environnement, CNRS-UPS-INPT, Toulouse, France, [7]Université Laval, Quebec City, QC, Canada, [8]Hydro Québec, Montréal, QC, Canada

Abstract First-order streams flowing through peatlands receive, carry and transform large amounts of organic carbon, methane (CH_4) and carbon dioxide (CO_2) but remain poorly documented. The objectives of this study were to (a) identify the origins of CO_2 and CH_4 (thereafter C-GHG for carbon greenhouse gases) in a peatland headwater stream, (b) determine the environmental factors driving C-GHG export and emissions, and (c) quantify C-GHG losses from this system and discuss its implications. Data were collected from eight sampling sites along a 3 km boreal peatland headwater stream (Eastern Canada) over the growing seasons 2019 and 2020. The studied stream was oversaturated in pCO_2 [min: 2,044; max: 23,306 µatm] and pCH_4 [14; 17,614 µatm]. A mass balance model showed that ~81% of in-stream CO_2 originated from porewater seepage while the remaining 17% and 2% originated from in-stream productivity and methane oxidation, respectively. Porewater seepage was concluded to be the primary source of CH_4. Seasonal dissolved C-GHG concentrations were negatively correlated with the peatland water table depth, suggesting an active release of carbon-rich peat porewater during the base flow. Nevertheless, greater C-GHG losses occurred during stormflow periods which acted as pulses with most of the C-GHG being shunted downstream. The sum of C-GHG export and emissions at our site was 8.08 gC m^{-2} y^{-1} with 86% being released to the atmosphere and 14% being exported downstream. Our study demonstrates that peatland headwater streams act as large sources of C-GHG and that precipitation events and topography control the magnitude of the fluxes.

Plain Language Summary Headwater streams are the inceptive fragment of the river network where a substantial quantity of organic carbon is released from the surrounding substrate. This terrestrial organic carbon can also be transformed into greenhouse gases (GHGs) such as methane and carbon dioxide. In the stream, those GHG can be either consumed, emitted to the atmosphere, or exported downstream. However, the respective contribution of those pathways is unknown. We sampled a stream draining a rain-fed peatland in Eastern Canada to describe and quantify its carbon GHG dynamics. We found higher concentrations in this stream than in most headwater streams but the total carbon emissions and export were comparable. Peatland streams typically have a low velocity and gentle slope which minimizes atmospheric gas release. We also found that concentrations were greater during the low flow period, potentially because carbon-rich porewater was released from the peat. However, greater export was reported during the few days of intense rain. The significance of this work is that GHG in headwater streams are spatially and temporally variable and controlled by the surrounding ecosystems, the intensity of rain events and the stream morphology. The inclusion of this variability will improve regional and global carbon budget estimates.

Key Points:

- Porewater seepage accounted for 81% of the carbon dioxide (CO_2) present in the stream, in-stream production and methane (CH_4) oxidation contributed to 17% and 2%
- 86.5% of the dissolved CO_2 and CH_4 was emitted to the atmosphere rather than exported downstream due to gases oversaturation and slow flow
- 46% of the CO_2 and CH_4 exported downstream occurred during the 10% period when water discharge rates were maximum, suggesting a pulse effect

Supporting Information:

Supporting Information may be found in the online version of this article.

Correspondence to:

P. Taillardat,
taillardat.pierre@nus.edu.sg

Citation:

Taillardat, P., Bodmer, P., Deblois, C. P., Ponçot, A., Prijac, A., Riahi, K., et al. (2022). Carbon dioxide and methane dynamics in a peatland headwater stream: Origins, processes and implications. *Journal of Geophysical Research: Biogeosciences*, *127*, e2022JG006855. https://doi.org/10.1029/2022JG006855

Received 15 FEB 2022
Accepted 15 JUN 2022

Author Contributions:

Conceptualization: Pierre Taillardat, Pascal Bodmer, Antonin Prijac, Laure Gandois, Michelle Garneau
Data curation: Pierre Taillardat, Pascal Bodmer, Alex Ponçot
Formal analysis: Pierre Taillardat, Pascal Bodmer
Funding acquisition: Alain Tremblay, Michelle Garneau
Investigation: Pierre Taillardat, Charles P. Deblois, Antonin Prijac, Khawla Riahi
Resources: Paul A. del Giorgio

1. Introduction

Despite their relatively small surface area at the global scale, the recognition of running waters as biogeochemical hotspots has been growing over the last two decades (Aufdenkampe et al., 2011; Battin et al., 2009; Cole et al., 2007; Duvert et al., 2018; Rosentreter et al., 2021). Streams and rivers receive, transform, and store carbon fixed by the terrestrial vegetation, while transporting and releasing a variable fraction to the atmosphere and downstream environments, respectively. Hence, excluding them from net ecosystem carbon budgets (NECB) often leads to an overestimation of ecosystem carbon sequestration (Dinsmore et al., 2010; Taillardat et al., 2020;

Visualization: Pierre Taillardat, Alex Ponçot
Writing – original draft: Pierre Taillardat, Pascal Bodmer
Writing – review & editing: Pascal Bodmer, Charles P. Deblois, Alex Ponçot, Antonin Prijac, Khawla Riahi, Laure Gandois, Paul A. del Giorgio, Marc André Bourgault, Alain Tremblay, Michelle Garneau

Webb et al., 2019). At the global scale, the lack of inclusion of aquatic carbon loss tends to overestimate bottom-up terrestrial carbon sink estimates. For instance, Butman et al. (2016) reported that the aquatic carbon processes offset about 27% of the terrestrial sink within the conterminous United States. This has serious implications since most countries intend to use nature-based climate solutions to reach carbon neutrality before the end of the century, as mentioned in the Paris Agreement (UNFCCC, 2015).

Headwater streams (i.e., first to third-order streams using the Strahler number) represent about 17% of the fluvial surface area but over 89% of the total stream and river length (Downing et al., 2012). Because of their extensive proximity to the adjacent land cover, headwater streams are disproportionally fueled by surface runoff and porewater seepage (i.e., subsurface discharge from the surrounding substrates and hyporheic zone), with solutes and particles from carbon-rich terrestrial ecosystems (Campeau et al., 2019; Hotchkiss et al., 2015). Therefore, headwater streams are commonly highly oversaturated in carbon dioxide (CO_2) and play a decisive role in the landscape carbon cycling despite their relatively limited surface area (Wallin et al., 2013). Headwater streams can also be supersaturated in methane (CH_4), although concentrations are more variable than CO_2 within and among streams (Rasilo et al., 2017; Stanley et al., 2016). The surrounding land cover is assumed to account for most of this variation (Aho & Raymond, 2019; Stanley et al., 2016) but oxidation processes occurring at the soil-stream interface (i.e., hyporheic zone) and in the stream also affect CH_4 (and consequently CO_2) concentration and composition (Rasilo et al., 2017).

In general, the carbon dynamics of headwater streams over time are still not well understood (Marx et al., 2017). The "pulse-shunt concept" was developed as a theoretical framework to incorporate episodic seasonal dynamics involving high organic matter export during large hydrological events occurring at low frequencies in headwater streams (Raymond et al., 2016). Whether this framework applies to streams draining peatlands and can be extended to describe the dynamics of carbon gases such as CO_2 and CH_4 remains to be clarified. In addition to surface runoff and porewater seepage from the surrounding land cover, other processes such as photochemical oxidation (hereafter photo-oxidation) and microbial mineralization occurring within the water column can also affect CO_2 concentration. Both processes convert organic carbon into CO_2. The first one, photo-oxidation, is an abiotic process that breaks down and oxidizes organic compounds through solar radiation (Granéli et al., 1998). This process, if predominant, would typically increase CO_2 concentrations during daytime. The second process, microbial mineralization, is related to in-stream metabolism. Streams can convert CO_2 into organic matter through Gross Primary Productivity (GPP) and release CO_2 via Ecosystem Respiration (ER). The sum of those two processes can help determine the stream Net Ecosystem Production (NEP = GPP − ER) and understand if metabolism acts as a source (NEP < 0) or sink (NEP > 0) of CO_2 within the stream. High GPP rates would typically lower CO_2 during the day as a result of photosynthesis and therefore counteract CO_2 production through photo-oxidation. A third process that produces CO_2 and consumes CH_4 in freshwater environments is methane oxidation mediated by methanotrophic bacteria (Hanson & Hanson, 1996), although a smaller fraction can also occur anaerobically (Schubert et al., 2011; Sivan et al., 2011). The CH_4 oxidizing process is predominantly dependent on temperature (Shelley et al., 2015) and CH_4 availability (Guérin & Abril, 2007).

One challenge that is particularly relevant for peatland streams is that diel patterns, typically explained by in-stream productivity (Attermeyer et al., 2021), appear to be less pronounced (e.g., Campeau, Bishop, et al., 2017; Campeau, Wallin, et al., 2017; Dawson et al., 2004). Additionally, studies that used carbon stable isotopes reported that the supersaturation of CO_2 and CH_4 is most likely a result of surface runoff and porewater seepage from the surrounding carbon-rich environment rather than in-stream metabolism (Campeau et al., 2018). While CO_2 could be affected by GPP (i.e., lower CO_2 concentrations during the afternoon) and thus follow a consistent diel pattern, it is not clear what would be the CH_4 diel dynamics, if any, and the main driving processes (Rasilo et al., 2017; Stanley et al., 2016).

Emissions to the atmosphere of CO_2 and CH_4 from streams are controlled by gas transfer velocity (k), gas solubility and gas concentrations in the air and water (MacIntyre et al., 1995). Since gas transfer velocity is considered to be rate-limiting for gas fluxes—and also because it generates the highest uncertainties since it is often predicted using empirical relationships (Zappa et al., 2007)—a lot of work has focused on improving the gas transfer velocity estimates in contrasting stream conditions. However, we note that most of the recent studies have been conducted in high altitude and high energy systems where the gas transfer velocity and associated C-GHG emissions are expected to be the highest (e.g., Clow et al., 2021; Hall & Madinger, 2018; Schelker et al., 2016; Ulseth et al., 2019; Whitmore et al., 2021). Other studies have examined the contribution of streams with low

gas transfer velocity but surrounded by carbon-rich environments such as wetlands. Aho and Raymond (2019) investigated the influence of wetlands on greenhouse gas (GHG) evasion from temperate streams and reported that GHG concentrations were higher in wetlands streams but that the emission of GHGs was not, when compared to forested streams, as a result of lower gas transfer velocity. Nevertheless, wetland-derived gases are assumed to ultimately evade to the atmosphere farther down the stream network (Aho & Raymond, 2019). Thus, gas transfer velocity may only control the timing of when GHGs from headwater streams evade while the concentration of gases influences the magnitude of GHGs emissions. Similarly, Aho et al. (2021) examined the concentration-discharge dynamics in temperate streams. Unlike all the other studied streams, both dissolved CO_2 and CH_4 concentrations did not decrease with increasing discharge. This suggests that wetlands, when hydrologically connected to streams, act as steady sources of GHGs. The paramount importance of lateral carbon inputs from wetlands to explain GHGs emissions from streams was also reported in Africa, such as the Congo River network (Borges et al., 2019) and the Nyong watershed (Moustapha et al., 2022), high altitude tropical wetlands (Schneider et al., 2020), but also in temperate and boreal peatlands (Billett & Harvey, 2013; Billett & Moore, 2008; Dinsmore et al., 2010). Considering the relatively flat topographies draining wetlands and the large carbon stocks they hold, particularly in peatlands, it is worth exploring their carbon GHG dynamics and identifying their biogeochemical specificities, in comparison to other headwater streams. This is of particular importance for CH_4 since about half of global CH_4 emissions are generated by aquatic environments but where local and global estimates are still highly uncertain (Rosentreter et al., 2021).

In this study, we aimed at understanding the functioning of peatland headwater streams. More specifically, we wanted to test the hypothesis that such streams are primarily fueled by peat-derived lateral porewater seepage and that they emit and export large amounts of CO_2 and CH_4. This study was designed to address the following three research objectives: (a) identify the origins of CO_2 and CH_4 in a peatland headwater stream based on concentrations and stable isotope data over multiple field campaigns; (b) determine the environmental factors driving CO_2 and CH_4 export and emissions using continuous measurements at seasonal and diel scales, including storm events; (c) quantify CO_2 and CH_4 losses from the studied peatland headwater stream, and discuss their potential implications at the ecosystem and regional scale. This study presents two complementary data sets. First, a spatial analysis of carbon dynamics conducted along the studied peatland headwater stream. Second, a temporal analysis of a 55-day long time series performed at the outlet of the stream.

2. Methods

2.1. Study Site

The study was conducted within the La Romaine watershed (Figure 1a), located in the Spruce-moss bioclimatic domain of the closed boreal forest of Eastern Canada (Payette et al., 2001). The regional 30-year normal (1990–2019) mean annual temperature, rainfall and snowfall are 1.5°C, 422 mm, and 589 mm, respectively (Environment Canada, https://climate.weather.gc.ca/historical_data/search_historic_data_e.html). The coldest and warmest months are January and July with mean daily temperatures of −13.9°C and 15.1°C, respectively. Average monthly positive temperature occurs from May to October.

We studied a first-order stream having its source within and flowing through an ombrotrophic peatland (Figures 1b, 50°31′N; 63°12′W, elevation: 108 ± 5 m above sea level; catchment area 1.18 km^2). While the entire length of the stream from its headwater to its outflow in the La Romaine River is around 15 km, we focused on the first 3 km stretch, which corresponds to the section that transits through the peatland exclusively (i.e., from source to peatland outlet; Figure 1b). The studied portion of the headwater stream flows along a northeast-southwest axis, through a dome-shaped bog complex covering 67% of its watershed (Electronic Supplemental Material Figure S1 in Supporting Information S1) following the local topography influenced by Canadian Shield bedrock and postglacial sandy sediments (the latter representing 8% of the total studied watershed; Figure S1 in Supporting Information S1).

The peatland has a patterned surface of alternating microforms characterized by hummocks, lawns, hollows, and pools. The surface vegetation follows the microform humidity gradient with *Sphagnum fuscum*, *S. capillifolium*, and *Cladonia rangiferina* on the hummocks, *S. magellanicum*, *S. rubellum*, *S. cuspidatum* and *Trichophorum cespitosum* on lawns and *S. majus* and *S. pulchrum* on hollows (Primeau & Garneau, 2021). Peat started to accumulate at 9070 calibrated years before the Present following postglacial Goldthwait sea retreat and maximum

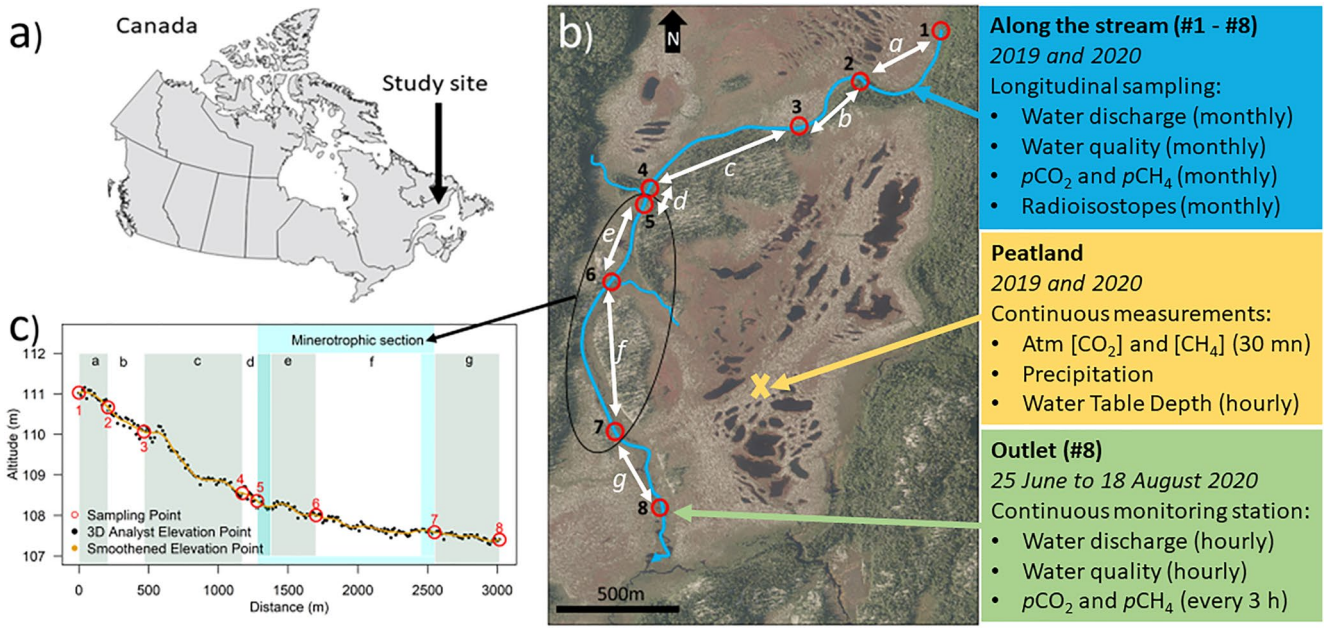

Figure 1. (a) Location of the study area in Canada; (b) aerial photograph of the study site with the headwater stream in blue and the sampling points indicated by red circles and a summary of the sampling strategy; (c) elevation gradient of the headwater stream from the most upstream sampling site (#1) to the outlet (#8) are indicated by letters (a–g).

peat depth reaches 440 cm. The long-term rate of carbon accumulation (LORCA) calculated by Primeau and Garneau (2021) was estimated at 35.5 g C m^{-2} y^{-1} with a total carbon stock of 200.7 ± 10.2 kt C.

Eight sampling points were selected to assess the biogeochemical variation along the stream. A sampling point was set whenever the adjacent land cover or stream hydrodynamics seemed to differ from upstream. Each sampling point was considered to be representative of a sub-catchment (Figure S1 in Supporting Information S1). Distance and elevation between sampling points were determined using a LiDAR image from 17 August 2004 (source: Hydro-Québec). The headwater stream and sampling points were drawn and pinned on ArcGIS v10.5.1 (Environmental Systems Research Institute, USA). Their respective elevations were extracted from the computed digital elevation model using the 3D analyst tool (Figure 1c). The elevation gradient was then smoothed using the loess function in R programming language (Core Team, 2021).

2.2. Sampling Strategy

The quantification of aquatic carbon GHG (C-GHG) fluxes requires a combination of hydrometeorological and geochemical analyses that are described below and summarized in Figure 1.

To describe the spatial and temporal variation in the partial pressure of CO_2 (pCO_2) and CH_4 (pCH_4) along the headwater stream, we collected samples across the eight sampling points from the stream source (point #1) until the last (point #8; Figure 1b), which is considered the outlet of the entire section of the strean considered in this study. The stream was separated into seven segments (a–g) (Figure 1c) used for mass balance calculations. Data collection was done during the snow-free seasons from June 2019 to September 2020, usually once a month. This accounted for a total of seven field campaigns during which all points were sampled within the same day, following the water flow direction (i.e., from upstream to downstream). To minimize possible disturbances, only one researcher was entering the stream for water flow and water depth measurements. At each sampling point, all samples were collected from the bank of the stream a few meters upstream from where the water flow measurements were taken. With this procedure, we minimized any artifact created from the potential stream disturbance. Additionally, a period of about 1 hr was left between the visit of the respective sampling points.

To describe pCO_2 and pCH_4 spatial and temporal variation at the stream outlet (point #8), hourly discharge rates, water quality as well as dissolved CO_2 and CH_4 concentrations were measured using a combination of automated equipment as described below.

2.3. Hydrometeorological Measurements

2.3.1. Stream Water Discharge

At each sampling point ($n = 8$, Figure 1b) along the stream, water depth and width were measured using a measuring tape. Water velocity through a cross-section was estimated using a portable flow velocity probe (Flo-mate model 2000, Marsh-McBirney Inc., USA). Measurements were taken transversely to the stream at 20-cm intervals. Level-discharge rating curves (Q; $m^3\ s^{-1}$) were calculated using cross-sectional flow velocity (V; $m\ s^{-1}$) and depth (m) multiplied by width (m) to determine the flooded vertical surface area (A; m^2) as described in Equation 1:

$$Q = V \,.\, A \tag{1}$$

At the outlet sampling point (#8), hourly discharge rates were monitored from 25 June 2019 to 18 August 2020. A 90° «V» notch weir was installed perpendicularly to the stream water flow (Figure S2 in Supporting Information S1). Water level was recorded every hour using Equation 1 a calibrated rugged acoustic distance sensor (SR-50A, Campbell Scientific, USA) connected to a data logger (CR1000, Campbell Scientific, USA) and (b) a water level pressure sensor (HOBO U20-001-004, ONSET, USA) installed at the bottom of the stream. Thomson's triangular-notch weir equation was used to convert water level into discharge (Shen, 1981).

2.3.2. Peatland Monitoring

A meteorological station connected to an eddy covariance system with a sonic anemometer (CSAT3, Campbell Scientific, USA), and InfraRed Gas Analyzers (IRGA) for CO_2, H_2O, and CH_4 measurements (LI-7200 and LI-77000, Li-Cor Biosciences, USA) was installed at about 600 m NW from the outlet (Figure 1b). Rainfall from a rain gauge (0.2 mm accuracy, HOBO RG3-M, Onset, USA) and atmospheric CO_2 and CH_4 concentrations were used in this study. Additionally, we measured water table depth using a water level pressure sensor (U20 Hobo, ONSET, USA) within a PVC pipe introduced at 2 m deep in the peat which was compensated from ambient atmospheric pressure using a second pressure sensor left at the site, aboveground (Figure 1b).

Peat porewater samples were collected during the field campaign in June, August, and September 2019. Two microforms, a hummock and a depression, respectively, were selected to account for spatial variation and samples were taken at 30 cm, 70 cm, and 100 cm below the peat surface. Water samples were collected using a peristaltic pump for dissolved CO_2 and CH_4 (triplicated samples). Dissolved oxygen (DO), pH, and porewater temperatures were measured using a multiparameter probe (WTW Multi 3620 IDS, Xylem Analytics, Germany).

2.4. Geochemical Measurements

2.4.1. pCO_2 and pCH_4 and Their Stable Isotopic Composition

The pCO_2, pCH_4, and stable isotope composition ($\delta^{13}C\text{-}CO_2$ and $\delta^{13}C\text{-}CH_4$) were determined using the headspace technique (modified from Rasilo et al., 2017). Triplicate samples were taken at each sampling point for every field campaign. Additionally, samples were taken every hour over a 24 hr sampling effort at the outlet section on 1 and 2 August 2019. Briefly, a 60-mL gas-tight plastic syringe was filled with 30 mL of surface water and 30 mL of hydrocarbon-free Ultrapure Zero Air (Praxair Canada Inc., Canada). The syringe was shaken vigorously for 1.5 min to equilibrate the water and air phases inside the syringe and the equilibrated headspace was transferred to a pre-evacuated 12 mL Exetainer glass vial (Labco International Inc., UK) and stored at ambient air temperature until analysis. Water temperature in the stream and the syringe after the equilibration were measured with a digital thermometer (Fisherbrand™ Traceable™, Fischer Scientific, USA). Samples were analyzed in the laboratory using a cavity ring-down spectroscopy (CRDS) analyzer (G2201-i, Picarro Inc, USA) equipped with a gas autosampler (SAM, OpenAutosampler Inc, Canada) to determine pCO_2, pCH_4, $\delta^{13}C\text{-}CO_2$, and $\delta^{13}C\text{-}CH_4$. The CO_2 and CH_4 isotopic data are reported in the standard data notation (δ) expressed in ‰ relative to the standard Vienna Pee Dee Belemnite. Gas standards (AlphagazTM Isotope Natural Air, Airgas, USA) were analyzed at the beginning, after 25 samples within each run, and at the end of each run to ensure consistency. High concentration

samples were diluted using Ultrapure Zero Air (Praxair Inc., Canada) to stay within the measurement guaranteed spec range of the analyzer (CO_2 = 380–2,000 ppm; CH_4 = 10–500 ppm; [Picarro Inc., 2016]). The pCO_2, pCH_4 and their respective stable isotopic signatures were corrected using the stream water in situ temperature and water temperature in the syringe after the equilibration.

From 25 June 2020 to 18 August 2020, a GHG automated monitoring system was installed at the outlet to measure water pCO_2 and pCH_4 every 3 hr starting at midnight every day. Water was sampled at a depth of 10 cm with a peristaltic pump and channeled into a gas equilibrator (Minimodule membrane contactors, Liqui-Cel, USA) for 30 min to allow equilibration of partial pressures between the water and air phase in the module lumen. The air phase circulated in a closed loop at a rate of 1 LPM with an air pump and flowed from the minimodule to a desiccant chamber and the analytical instruments. Gases were measured with a non-dispersive infrared sensor (Li-Cor Li-850, USA; 0–20,000 ppm; 2%–4% accuracy) for pCO_2 and with a Tunable Diode Laser Spectroscopy sensor (TDLS; Axetris LGD Compact A, Switzerland; 0–100 ppm, precision ≤0.8 ppm) for pCH_4. Although calibrated between 0 and 100 ppm, the TDLS was tested at concentrations up to 10,000 ppm in the lab and was accurate to 5%. The system also measured air temperature, water temperature, air loop pressure, and relative humidity. Data were recorded by a data logger (CR1000x, Campbell Scientific, USA) at the end of each measuring cycle for a total of eight measurements per day. The pCO_2 and pCH_4 (ppm) were converted to concentrations (μM) based on water temperature and gas solubility coefficient from Weiss (1974) for CO_2 and Lide (2007) as described in Goldenfum (2010).

DO, water temperature, pH, and specific conductivity were measured using a multiparameter probe (EXO2, Yellow Springs Instruments, USA) whenever pCO_2 and pCH_4 samples were collected during both the spatial sampling periods and throughout the continuous measurements at the outlet (with a reading timestamp every hour). Similarly, samples for dissolved organic carbon (DOC) concentration analysis were filtered using pre-burned GF/F filters (Whatman, USA), acidified to pH 2 using 1 M HCl and stored in 40 mL glass vials. Analyses were performed using the catalytic oxidation method followed by non-dispersive infrared (NDIR) detection of produced CO_2 (TOC analyzer TOC-L, Shimadzu, Japan) with a limit of quantification of 0.1 mg C L^{-1}. Certified materials (ion 915 and ion 96.4, Environment and Climate Change Canada, Canada) were included in the analytical loop, and the recovery was >95% of the certified value.

2.4.2. Aquatic Flux Determination

Carbon dioxide and methane downstream exports by streamflow (mol h^{-1}) were estimated using an "Eulerian" approach by multiplying the water flow (m^3 h^{-1}) with the gas concentration (mol m^{-3}) at each sampling point (e.g., Taillardat et al., 2018).

Water-air CO_2 and CH_4 fluxes were measured using the drifting chamber method (Lorke et al., 2015) during the field campaigns of June, August and September 2019. A custom-built floating chamber (0.157 m^2, 0.042 m^3) was connected to a Cavity Ring-Down Spectroscopy (CRDS) GHG analyzer (GasScouter, Picarro Inc, USA) with a reading frequency of 1 s (Goldenfum, 2010; Mannich et al., 2019; Rosentreter et al., 2017). Within the chamber headspace, a temperature sensor (HOBO Pendant UA-002-08 Temperature/Light, ONSET, USA) was installed to take measurements every 10 s. For each site, five flux measurements were performed for 5 minutes each and calculated following Equation 2:

$$F = \left(S_{pCO_2} \text{ OR } S_{pCH_4}\right) \cdot \frac{V}{R \cdot T_{\text{air chamber}} \cdot A} \quad (2)$$

where F is the water-air CO_2 or CH_4 flux (mmol m^{-2} s^{-1}); S_{pCO_2} or S_{pCH_4} is the slope of CO_2 or CH_4 inside the chamber over time (ppmV s^{-1}); V is the total volume of the flux chamber + tubing (m^3); R is the ideal gas constant (atm m^3 K^{-1} mol^{-1}); $T_{\text{air chamber}}$ is the absolute air temperature in the chamber (K); and A is the water surface covered by the chamber (m^2). The slopes were calculated using linear regressions. Only regressions with an $R^2 \geq 0.89$ were used to calculate F.

2.4.3. Gas Transfer Velocity Determination

The gas transfer velocity (k; m d^{-1}) of CO_2 and CH_4 were derived using Equation 3:

$$k = \frac{F \cdot 3.6}{(K_0 (p_{\text{water}} - p_{\text{air}}))} \quad (3)$$

where F is the flux measured with the floating chamber expressed in mmol m^{-2} s^{-1} (Equation 2), K_0 is the solubility coefficient expressed in mol L^{-1} atm $^{-1}$ (Weiss, 1974) and partial pressure differences between water (p_{water}) and atmosphere (p_{air}) in µatm.

Based on field measurements during the campaigns of June, August, and September 2019, k was determined for each sampling point ($n = 8$), combining direct flux chamber measurements (see Section 2.4.3) and dissolved CO_2 and CH_4 using the headspace technique (see Section 2.4.2). For sampling periods when only dissolved CO_2 and CH_4 samples were collected (i.e., no aquatic flux chambers), the median values specific to each sampling point were used.

The k values were also normalized to k_{600} values, which is the k at 20°C in freshwater equivalent to k at a Schmidt number of 600 using:

$$k_{600} = k \,.\, ({}^{S_c}/_{600})^{n} \tag{4}$$

where S_c is the Schmidt number of a gas at a given temperature (Wanninkhof, 1992). We used $n = 0.5$ for wind speed >3 m s^{-1} (Goldenfum, 2010).

2.4.4. In-Stream Metabolism

The rates of ecosystem metabolism were estimated for the period from 25 June to 18 August 2020 based on a Bayesian inverse model from a single-station (point #8; Figure 1b) diel DO change, where a change in O_2 concentration is a function of GPP, ER, and water-air gas exchange $\left(K_{O_2}\right)$ (Hall & Hotchkiss, 2017). Daily estimates of GPP, ER, and $K_{600_d\_O_2}$ were derived using the R package *StreamMetabolizer v0.12.0* (Appling, Hall, et al., 2018; Appling, Read, et al., 2018) using the following equation:

$$\frac{dO_{i,d}}{dt} = \left(\frac{GPP_d}{\overline{z}_{i,d}} + \frac{PAR_{i,d}}{\overline{PAR}_d}\right) + \left(\frac{ER_d}{\overline{z}_{i,d}}\right) + f_{i,d}\left(K_{600_d-O_2}\right)\left(O_{sat_{i,d}} - O_{i,d}\right) \tag{5}$$

where $O_{i,d}$ is the modeled oxygen concentration on day d at time index i (i.e., 1 hr), and $dO_{i,d}$ / dt is a rate of DO concentration change. GPP_d, ER_d, and $K_{600_d\_O_2}$ are the three daily parameters fitted by the model: GPP_d and ER_d are daily average rates of GPP and ER, respectively (g O_2 m^{-2} d^{-1}), while $K_{600_d\_O_2}$ is a daily average value of the standardized gas transfer velocity (k_{600} in m d^{-1}) divided by stream depth (in m). The other variables are model inputs: $\overline{z}_{i,d}$ is the stream depth (m) averaged over the width and length of the specific stream section; $PAR_{i,d}$ is the photosynthetic photon flux density (µmol photons m^{-2} d^{-1}); PAR_d is the daily mean of observed $PAR_{i,d}$; $f_{i,d}\left(K_{600_d\_O_2}\right)$ is a function that converts daily mean $K_{600_d\_O_2}$ to an O_2-specific, temperature-specific gas exchange coefficient ($K_{O_{2_{i,d}}}$, d^{-1}), and $O_{sat_{i,d}}$ is the theoretical saturation concentration of O_2 if the water and air were in equilibrium. A threshold of $r^2 \geq 0.9$ of the Pearson correlation coefficient between modeled and measured O_2 values were fixed to include or exclude daily GPP, ER and NEP estimates.

The $K_{600_d\_O_2}$ was estimated from the night-time regression method using the function *metab_night*. Photosynthetically active radiation (PAR) based on geographic location was estimated using the *calc_light* function. To compare CO_2 consumed by GPP with observed CO_2 emissions, we assumed that 1 mol of O_2 is exchanged by 1 mol of CO_2 (e.g., Crawford et al., 2013; Rocher-Ros et al., 2020).

2.5. Mass Balance Models

For each of the seven segments (a–g; Figure 1c), a mass balance was applied for CH_4 and CO_2, respectively. Inputs for CH_4 are represented by the input from upstream (F_{in} mol d^{-1}) while the output accounted for the sum atmospheric emission (F_a mol d^{-1}), downstream export (F_{out} mol d^{-1}) plus methane oxidation (F_{ox} mol d^{-1}). The sum of the input and the three outputs equal a residual (F_{res}; mol d^{-1}) to close the mass balance, which can be assumed to be porewater seepage (from peat porewater or the hyporheic zone):

$$F\_CH_{4_{res}} = F_{CH_{4_a}} + F_{CH_{4_{out}}} + F_{CH_{4_{ox}}} - F_{CH_{4_{in}}} \tag{6}$$

Aerobic methane oxidation (F_{ox}) in the water column was determined using a stable isotope mass balance, based on stable isotopic discrimination during microbial CH_4 consumption adapted from Thottathil et al. (2018).

Because CH_4 oxidation varies throughout the stream, we used segment-specific δ^{13}C-CH_4 isotopic values from field collection to remain consistent with our mass balance approach. The changes in the δ^{13}C-CH_4 signature between the different segments ($\delta^{13}CH_{4_{stream}}$) relative to the source of methane (peat porewater; $\delta^{13}CH_{4_{PW}}$) is associated with the kinetic isotopic effect (also referred as isotopic fractionation). More specifically, the preferential consumption of ^{12}C over ^{13}C during CH_4 oxidation can be used to estimate the fraction of CH_4 being oxidized (f_{ox}). We used the open-system model at steady state (Equation 7) to calculate f_{ox}:

$$f_{ox} = \left(\delta^{13}CH_{4_{stream}} - \delta^{13}CH_{4_{PW}}\right) / ((\alpha - 1).1000) \quad (7)$$

where α is the isotopic fractionation factor; We used a α value of 1.020, similar to what Thottathil et al. (2018) used for surface waters.

Inputs for CO_2 are represented by the sum from upstream ($F_{in;}$ mol d^{-1}), in-stream NEP (F_{NEP}; mol d^{-1}), and methane oxidation (F_{ox}; mol d^{-1}) while the output accounted for the total atmospheric emission (F_a; mol d^{-1}) plus downstream export (F_{out}; mol d^{-1}). The sum of those three inputs and two outputs generated a residual (F_{res}; mol d^{-1}) which represents porewater seepage:

$$F_{res} = F_{in} + F_{NEP} + F_{ox} - F_a - F_{out} \quad (8)$$

We highlight a few assumptions made for this model. First, In-stream NEP was estimated for segment g (as described in Section 2.4.4) and its value was applied to all segments. Second, photo degradation was considered to be intrinsically embedded in F_{NEP} since both processes (i.e., metabolism and photo degradation) consume ambient stream O_2 and generate CO_2 in the stream. The relative proportion of the two processes is difficult to discriminate since both are oxidizing the same pool of DOC and therefore generate a CO_2 with a similar δ^{13}C-CO_2 signature. Third, the mass balance models assume a steady state in which the concentrations of CO_2 and CH_4 remain constant within each segment so that inputs and outputs match and the budget is closed (Rasilo et al., 2017).

The unit in which the mass balance models are presented is in mole per day. While we acknowledge that this unit may not be the most appropriate for comparison with the literature, it is the most convenient one to upscale our segment results to the stream scale. For instance, the stream atmospheric emission is the sum of all the segments in mol d^{-1} while for the downstream export, only the outflow at the outlet matters for the stream budget. We also highlight that the normalization area can differ depending on the variable we are interested in. For example, it is meaningful to present the atmospheric emission, internal production, and methane oxidation in mmol m^{-2} of stream area d^{-1} while for the downstream export, it is more relevant to present this value in mmol m^{-2} of the drained catchment d^{-1}. This is another reason why we decided to present the mass balance in mol d^{-1}.

2.6. Seasonal Estimate

Losses of CO_2 and CH_4 at the catchment scale, either to the atmosphere or downstream, were calculated by summing the estimate of emission rates of segments a–g and the downstream export from the outlet. Our study design combined a detailed spatial characterization of the CO_2 and CH_4 dynamics along the stream from manual sampling (Approach 1; see Section 2.4.1 paragraph 1) and a continuous time series at the outlet only (Approach 2; see Section 2.4.1 paragraph 2). Both approaches had strengths and drawbacks. Approach 1 provided an accurate description of the spatial variation (i.e., eight sampling points) but was only done during seven dates/field visits. Approach 2 offered a continuous high-resolution time series (i.e., measurements every 3 hr over 55 days), but the set of equipment was only deployed at the outlet. Thus, a model was developed to integrate those two approaches by comparing the C-GHG loss value obtained during the 2 days when data were available for both approaches (18 June and 27 August 2020). The model provides a correction factor that can be applied to the outlet values (Approach 2) during the days when no field visit took place. This allowed us to derive an integrated estimate of CO_2 and CH_4 emissions along the stream during the growing season of 2020.

Approach 1 is based on the section-specific dissolved CO_2 and CH_4 concentrations, k value, and drainage surface area following Equation 3, all determined from manual sampling. The total stream emission (F_GHG_{app1}; mol d^{-1}) is calculated by summing up the emissions from the seven stream segments:

$$F\_GHG_{app1} = [dGHG]_2 . k_2 . ss_a + [dGHG]_3 . k_3 . ss_b + [dGHG]_4 . k_4 . ss_c + [dGHG]_5 . k_5 . ss_d + [dGHG]_6 . k_6 . ss_e + [dGHG]_7 . k_7 . ss_f + [dGHG]_8 . k_8 . ss_g \quad (9)$$

where $[dGHG]_x$, expressed in µM, is the CO_2 or CH_4 partial pressure differences between water (p_{water}; µatm) and atmosphere (p_{air}; µatm) multiplied by the gas solubility coefficient (mol L^{-1} atm^{-1} (Weiss, 1974)). The p_{water} were measured at the respective sampling point indicated as subscript (2–8); p_{air} was taken from the eddy covariance tower located at the center of the peatland (Figure 1); k (m d^{-1}) is the gas exchange coefficient calculated at the sampling point indicated as subscript *(2 to 8)*; ss (m^2) is the stream surface area for the stream segment indicated as subscript (a–g).

Approach 2 is the total stream emission (F_GHG_{app2}; mol d^{-1}) calculated following Equations 2 and 3 based on automated measurements at the outlet and its respective k value. In this scenario, the concentrations $[dGHG]$ and k values were those from the outlet sampling point (#8). The resulting fluxes were then upscaled to the total upstream surface area:

$$F\_GHG_{app2} = [dGHG]_8 . k_8 . (ss_a + ss_b + ss_c + ss_d + ss_e + ss_f + ss_g) \quad (10)$$

The calculation that integrates spatial variation during the long-term continuous measurements at the outlet is based on the ratio between emission values from Approach 1 and Approach 2 during the two overlapping measurement days as presented in Equation 11:

$$F\_GHG_{index} = \frac{F\_GHG_{app2}}{F\_GHG_{app1}} \quad (11)$$

Thus, to derive a CO_2 and CH_4 emission budget for the whole stream between June 25 and 18 August 2020, that accounts for both spatial and temporal variation within the stream, we used Equation 12:

$$F\_GHG_{stream} = F\_GHG_{app2} . F\_GHG_{index} \quad (12)$$

The seasonal flux estimate was then normalized to (i.e., divided by) the catchment area in mmol m^{-2} y^{-1}.

2.7. Data Processing and Statistical Analysis

All data processing was done using R version 4.0.2 (Core Team R, 2021). The uncertainties presented in this paper are related to the interquartile range ($Q3$–$Q1$) unless specified. To quantify and express seasonal variation of DO, CO_2, and CH_4, data treatment was adapted from Tunaley et al. (2018). Daily amplitude was determined by subtracting the daily moving median of 24 hr from the measured values (i.e., 1 day equals one median value). Furthermore, we used linear models (LMs) to simultaneously test the effect of site and sampling period on pCO_2 and pCH_4, respectively ($pCO_2 \sim$ site + period; $pCH_4 \sim$ site + period). All models were followed by a model validation as well as checking the residuals for normal distribution and homogeneity of variances. The classification of "stormflow" as opposed to "base flow" was based on a 30-day moving average of water discharge values. Periods were considered as stormflow if discharge exceeded the 70th percentile of the monthly period (adapted from Dinsmore, Billett, et al., 2013; Dinsmore, Wallin, et al., 2013).

3. Results

3.1. Spatial Variation

3.1.1. pCO_2 and pCH_4

Over the measurement period, water discharge at the outlet was on average 18.4 L s^{-1} with 82% of the measurements being <25 L s^{-1} (Figure S3 in Supporting Information S1). All sampling days along the stream occurred during base flow periods except in September 2019 (Figure S3 in Supporting Information S1). Discrete samples ranged within one order of magnitude for pCO_2 (2,044–23,306 µatm) and three orders of magnitude for pCH_4 (14–17,614 µatm; Figure 2). For both gases, a strong spatial heterogeneity but a consistent pattern between

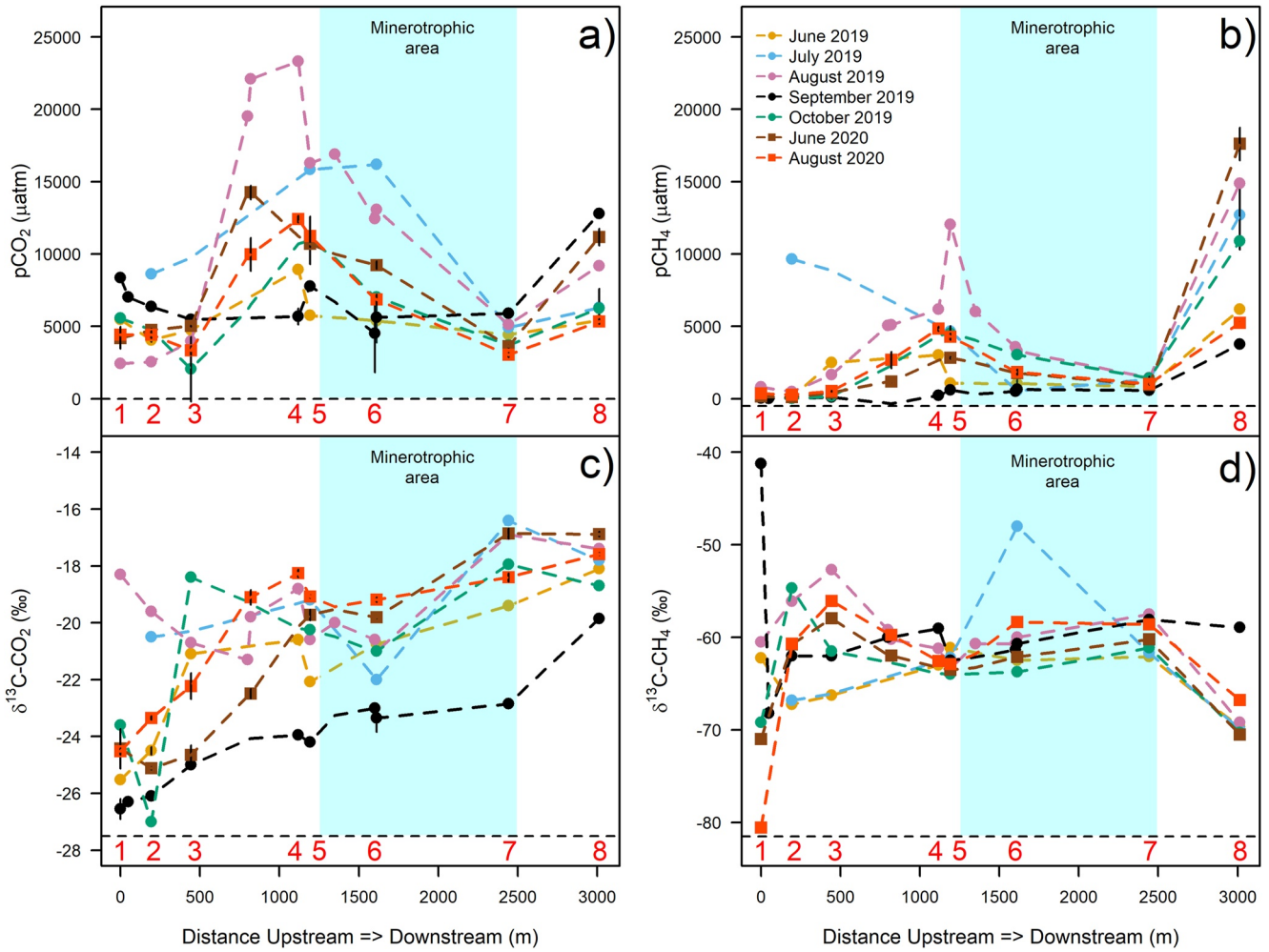

Figure 2. Partial pressure of carbon dioxide (pCO_2) and $\delta^{13}C$-CO_2 (panels a and c), and partial pressure of methane (pCH_4) and $\delta^{13}C$-CH_4 (panels b and d) measured along the stream (upstream to downstream = left to right). Different colors represent the different sampling periods. The blue background shows the section where the stream is flowing through minerotrophic conditions. The red numbers refer to the sampling points along the stream as in Figure 1. Data are presented as the median ± inter quartile range of the triplicate, when available.

sampling periods was observed (Figure 2). In particular, spatial variation in pCO_2 and pCH_4 along the stream continuum was significantly greater than the seasonal fluctuations (LM pCO_2: site, $p < 0.001$, period, $p = 0.08$; LM pCH_4: site, $p < 0.001$; period, $p = 0.03$). At the upstream source point (#1), values ranged from 2,430 µatm to 8,366 µatm for pCO_2 and from 28 to 813 µatm for pCH_4. Those values increased up to sampling point #5, reaching a maximum of 23,306 µatm and 12,048 µatm for pCO_2 and pCH_4, respectively (Figure 2). From point #5 to point #7, values decreased (Figure 2). At point #7, values were close to the most upstream point (#1), ranging from 3,035 to 5,908 µatm and 584 to 1,447 µatm for pCO_2 and pCH_4, respectively. This decrease occurred in a section where the stream flows between a rocky outcrop and sandy soils (Figure 1b). A multi radioisotopes analysis (^{222}Rn, ^{223}Ra, ^{224}Ra; Supplementary Methods 1 in Supporting Information S1) of water samples revealed that the area between #5 and #7 was the one with the highest radioisotope concentrations—an indicator of groundwater inputs or water in contact with mineral rather than peat (Figure S4 in Supporting Information S1) which was confirmed by the surrounding minerotrophic vegetation cover. An exploration to find groundwater seepage sources was conducted but no evidence of any source was found with the greatest radon concentration, up to 55,781 Bq m^{-3}, nearby the stream and within the sand deposit.

Between points #7 and #8, values increased again to reach concentrations as high as 12,784 and 17,614 µatm for pCO_2 and pCH_4, respectively (Figures 2a and 2b). This clear shift in pCO_2 and pCH_4 between those two points (i.e., #7 and #8) was reflected in the CH_4 stable isotopic values. A distinct depletion was found in the $\delta^{13}C$-CH_4

isotopic signature, from −60.21 ± 3.06‰ (median ± interquartile range) in #7 to −69.72 ± 2.11‰ at point #8 (Figure 2d, the latter having values much closer to the peat porewater endmember of −77.20 ± 3.58‰ (Table S1 in Supporting Information S1). $\delta^{13}C\text{-}CO_2$, on the other hand, showed systematic enrichment from upstream (#1: −24.48 ± 1.46‰) to downstream (#8: −17.80 ± 1.52), although a slight decrease was observed around site #5 (−20.25 ± 2.27‰; Figure 2c).

Samples collected in September 2019 diverged from those collected during the other sampling periods (Figure 2). The lowest pCH_4 and $\delta^{13}C\text{-}CO_2$ values were measured at this time at all sampling sites. The September 2019 sampling was carried out immediately after a major rain event and before the discharge peak (Figure S3 in Supporting Information S1). These hydrological conditions seem to have influenced pCO_2 and pCH_4 as well as other physicochemical parameters (Figure S5 in Supporting Information S1). A greater water discharge, DOC concentrations, and lower pH were measured at all sampling sites during this period (Figure S5 in Supporting Information S1).

The pCO_2 and pCH_4, as well as isotopic signatures values at each sampling site compared to the ones of the porewater sampling and point #8 was closest to the peat end member (i.e., peat porewater values in Table S1 in Supporting Information S1). The pCO_2 and pCH_4 in the peat porewater reached values as high as 87,318 and 304,993 µatm, respectively (Table S1 in Supporting Information S1). The ratio pCO_2 to pCH_4 was about 8 in the peat porewater but ranged from 70 to 512 along the surface stream waters, except for point #8 where the value was 17 (Table S1 in Supporting Information S1). The stable isotopic values of peat pore water showed very heavy signatures for $\delta^{13}C\text{-}CO_2$ [range: −9.95‰; −0.20‰] and very depleted signatures for $\delta^{13}C\text{-}CH_4$ [range: −82.45‰; −68.50‰].

3.1.2. Gas Emission

The CO_2 and CH_4 fluxes were calculated based on discrete samples collection along the stream and the site-specific gas transfer velocity k ($n = 55$) were determined using the aquatic flux measurements and reported here as k_{600}. The $k_{600\_CO_2}$ and $k_{600\_CH_4}$ ranged from 0.67 to 5.86 m d^{-1} and 0.00 to 6.51 m d^{-1}, respectively. Throughout the stream, the highest $k_{600\_CO_2}$ and $k_{600\_CH_4}$ were consistently measured at sampling point #7 (median = 4.27 and 5.24 m d^{-1}, respectively) while the lowest $k_{600\_CO_2}$ and $k_{600\_CH_4}$ were reported at point #8 (1.09 m d^{-1} and 1.19 m d^{-1}, respectively; Table S1 in Supporting Information S1).

The spatial distribution of CO_2 and CH_4 fluxes were split into three groups. The first group (sampling points #1–#3) represented the low emissions segment with median fluxes per sampling site between 206.64 and 227.27 mmol m^{-2} of stream area d^{-1} and 0.20–0.85 mmol m^{-2} of stream area d^{-1} for CO_2 and CH_4, respectively (Table S1 in Supporting Information S1). The second group (sampling points #4–#7) accounted for the high emission segment with fluxes ranging from 583.44 to 991.92 mmol m^{-2} d^{-1} and 6.35 to 13.85 mmol m^{-2} d^{-1} for CO_2 and CH_4, respectively (Table S1 in Supporting Information S1). The last group represented the remaining point #8 (i.e., outlet) which had opposite behavior for CO_2 and CH_4 emissions. The median CO_2 emission (305.76 mmol m^{-2} d^{-1}) was closer to Group 1 (i.e., low emission value) while the CH_4 emissions at point #8 were higher than in any other sampling site along the stream with a median value of 16.02 mmol m^{-2} d^{-1} (Table S1 in Supporting Information S1). The variation measured between the sampling periods was small relative to spatial variation along the stream.

3.1.3. In-Stream Metabolism

The determined $k_{600\_O_2}$ used in the metabolism model ranged from 1.02 to 3.22 m d^{-1} which is within the same order of magnitude as measured $k_{600\_CO_2}$ and $k_{600\_CH_4}$ presented in the above section. A total of 16 out of 55 days had a satisfying Pearson correlation coefficient between modeled and measured O_2 (see Section 2.4.4). All days had negative NEP (ER > GPP), ranging from −275.75 to −71.67 mmol m^{-2} d^{-1} (Table S2 in Supporting Information S1). Therefore, in-stream metabolism was a net source of CO_2 to the stream, rather than a sink.

3.1.4. Methane Oxidation

We used an isotopic mass-balance approach to determine the fraction of the CH_4 that has been oxidized (i.e., F_{ox}) for each stream section (Equation 7). This approach suggested that between 38% and 87% of the dissolved methane had been oxidized, depending on the subsection. This represents a methane oxidation flux (i.e., loss of CH_4 and gain of CO_2) of 3.4 mmol m^{-2} of stream d^{-1} (segment d) to 350.8 mmol m^{-2} of stream d^{-1} (segment c; Table S1 in Supporting Information S1).

3.1.5. Downstream Export

Median CO_2 and CH_4 downstream export from the stream outlet were 585.61 and 27.44 mol d^{-1}, respectively. When normalized by the catchment area (i.e., 1.18 km^2), values were 0.50 mmol m^{-2} d^{-1} and 23.25 µmol m^{-2} d^{-1} for CO_2 and CH_4, respectively.

3.1.6. CO_2 and CH_4 Mass Balance Along the Stream

Mass balance calculations along the different sections of the stream provided information on the origins and fate of CO_2 and CH_4 in the stream. The water discharge mass balance only confirmed that the stream was draining the catchment with a maximum discharge rate of 1,382.4 m^3 d^{-1} at the outlet (Figure 3) The CH_4 mass balance model was simpler than the CO_2 mass balance model since it included only two inputs (i.e., upstream inflow and lateral porewater seepage) and three outputs (atmospheric emission, methane oxidation and downstream export; Figure 3). It is meaningful to present CH_4 first since methane oxidation is a loss of methane that gets converted into CO_2 and therefore becomes a gain of CO_2 into the mass balance model (Figure 3). Our mass balance model at the stream scale suggests that only 19% of the methane input was exported downstream from the outlet station (27.4 mol d^{-1}) while methane oxidation and atmospheric emission represented 43% and 38% of the total average CH_4 loss, respectively. This means that most of the methane present in the stream is quickly oxidized or released to the atmosphere. The proportions of the processes were consistent among the segments except for the last segment *g* where porewater seepage represented a larger input in quantities as high as 61.1 mol d^{-1}, in comparison to upstream inflow (Figure 3).

Regarding CO_2, the mass balance model reported that porewater seepage accounted for 81% of the CO_2 present in the stream while in-stream production (represented by NEP) and CH_4 oxidation were minor sources contributing to 17% and 2%, respectively. Similar to CH_4, the CO_2 downstream export from the outlet represented a minor loss (15%) while most of the CO_2 was released directly to the atmosphere (85%).

A model was developed to estimate CO_2 and CH_4 losses from the peatland stream (Figure 3). As reported above, we measured the mass of CO_2 and CH_4 emitted to the atmosphere and exported downstream for 7 days of the seven segments during the period June 2019 to October 2020 (Figure 3). We conducted a comparative analysis to determine how much CO_2 and CH_4 emission would have been over- or underestimated if we would have only taken samples at the outlet instead (Table S3 in Supporting Information S1). Our analysis suggests that if we simply upscaled atmospheric emissions at the outlet section to the whole stream (F_GHG_{app2}) rather than integrating upstream spatial heterogeneity (F_GHG_{app1}), we would have underestimated CO_2 emissions by over 50%, and overestimated CH_4 emissions by the same magnitude (Table S3 in Supporting Information S1). This bias is based on the lower k_{600}, lower CO_2 and higher CH_4 concentrations reported at the outlet when compared to the other sampling sites along the stream (Figure 2). Integrating the sampling site variation is important for an accurate seasonal C-GHG budget as presented in the following section.

3.2. Temporal Variation

Because CO_2 and CH_4 values presented in µatm are directly affected by daily temperature variation, which was important at our stream site, in this section we present concentration values in µM to highlight metabolism processes rather than the physical interdependence between gas saturation and water temperature. Continuous measurements of dissolved CO_2 and CH_4 at the stream outlet (sampling point #8 in Figure 1) showed diverging trends. Dissolved CO_2 had a limited seasonal variation (min = 238.4; max = 425.9 µM) but high median diel amplitude (46.2 ± 6.2 µM) while dissolved CH_4 had a high seasonal variation (min = 2.0; max = 13.3 µM) and minimal, although still measurable, median diel amplitude (1.0 ± 0.5 µM; see Figure 4 for seasonal variation and Figure 5 for diel variation).

3.2.1. Seasonality

Over the 55 days of continuous measurements, the highest concentrations were measured over the period from 5 July to 26 July 2020, before the most important rain event of the season occurred (Figure 4). CO_2 and CH_4 concentrations decreased after rain events, often in parallel with increases in water discharge (Figure 4). This was particularly obvious following the rain events from 8 to 13 July 2020 (32 mm) and 27 to 31 July 2020 (74 mm). Water table depth (WTD) and CO_2 concentrations over the time series appeared to mirror each other, with higher CO_2 concentrations occurring at lower WTD. The same was true for CH_4, although the patterns were

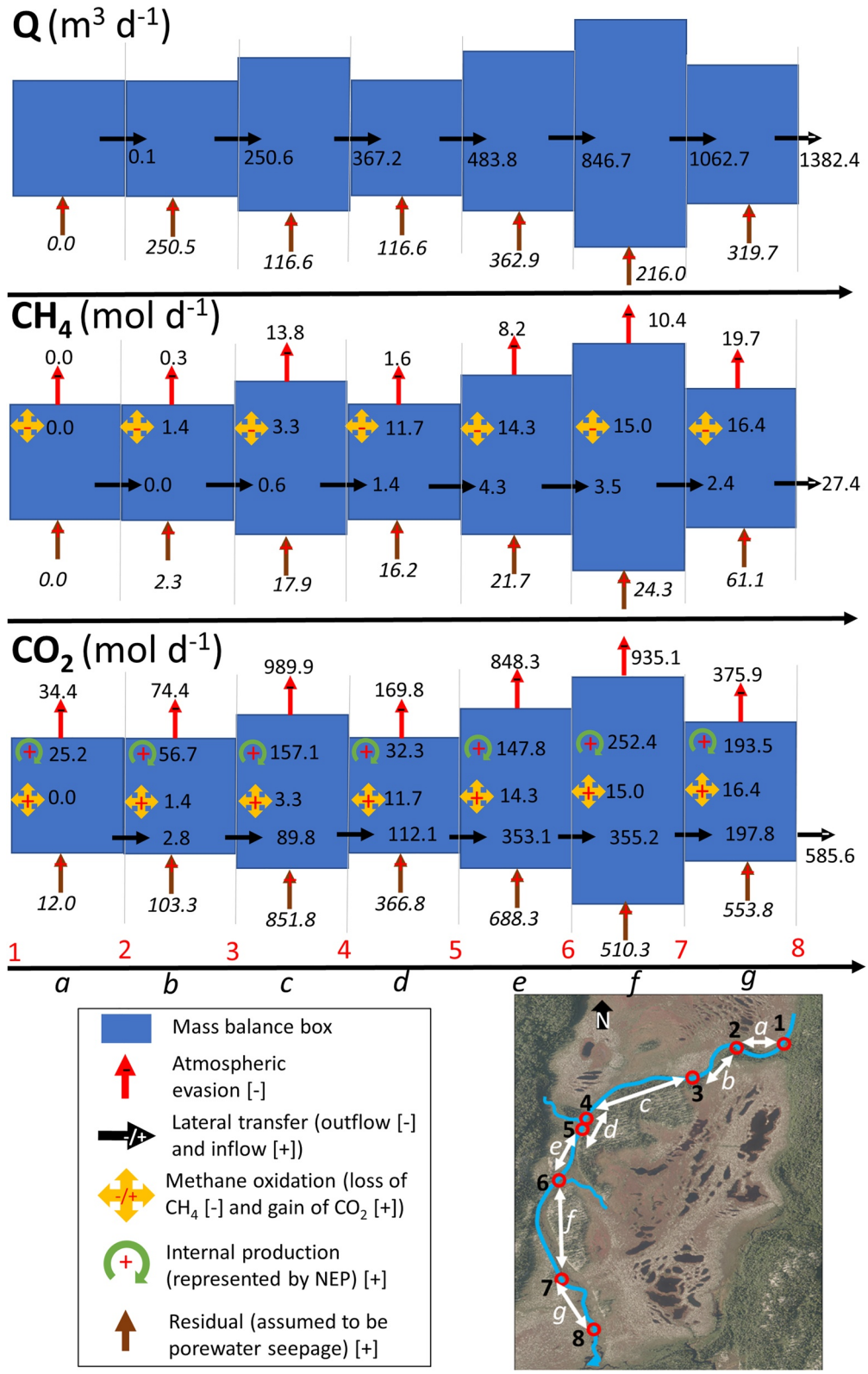

Figure 3. Mass balance model within and among the different stream segments for water discharge (Q in $m^3\ d^{-1}$), methane (CH_4 in mol d^{-1}) and carbon dioxide (CO_2 in mol d^{-1}). Note the sign in each arrow that indicates if the process act as a mass balance gain or loss.

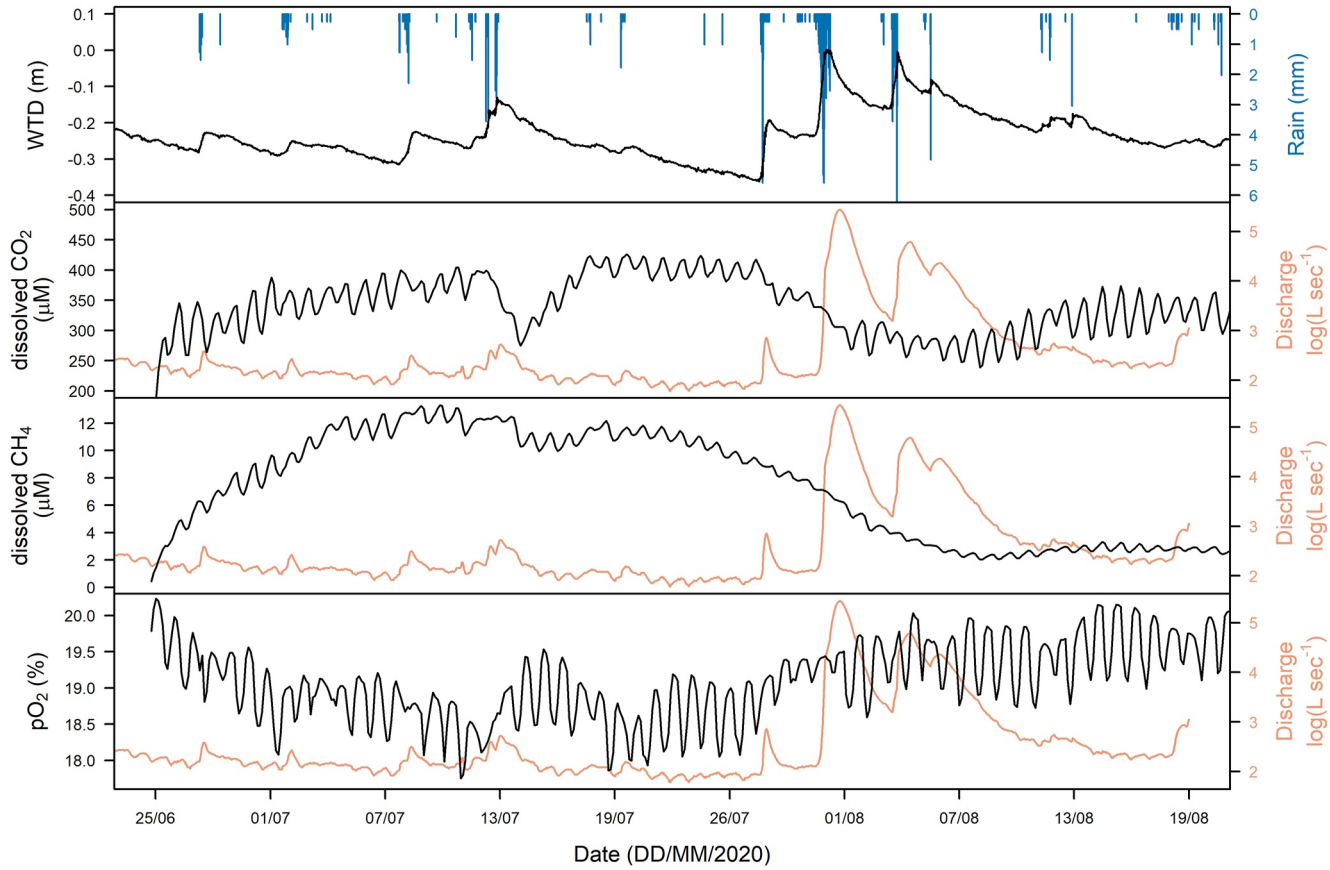

Figure 4. Time series measurements of rainfall, peatland water table depth (WTD), dissolved carbon dioxide (CO_2), dissolved methane (CH_4) and dissolved oxygen, and water discharge (in log[L s^{-1}]) at the stream outlet (=sampling point #8 in Figure 1 for the period 25 June 2020–18 August 2020.

not as coupled as for CO_2 (Figure 4). Based on WTD, the time series could be split into a "low-WTD period" for the period from 25 June to 27 July (<−0.2 m) and a "high-WTD period" (>−0.2 m) for the remaining period (Figure 4). A low-WTD period would correspond to high dissolved CH_4 concentrations and vice versa (Figure 4). No response in DO rates was observed in relation to water table variation but, generally, a high diel amplitude was detected except for the rainy days (Figure 4).

3.2.2. Diel Cycles

In 2020 during no rain periods, a clear diel pattern was measured at the outlet with minimum concentrations for CO_2 and CH_4 consistently measured in the afternoon (12:00–18:00; Figures 5b and 5c), even though variations were less distinct in August, particularly for CH_4. An opposite trend was measured for DO, δ^{13}C-CO_2 and δ^{13}C-CH_4 with a peak in the afternoon (Figures 5a, 5d and 5e).

3.2.3. Relationships With the Environmental Variables

A multilinear regression (MLR) approach was initially used to identify parameters influencing dissolved CO_2 and CH_4 variation at the seasonal time scale (not shown). The results of the MLR analysis suggest that WTD was the single main variable, with greater CO_2 and CH_4 concentrations when the water table was lower. Best linear regression models were found between CO_2 and WTD when the latter was averaged over the 7 days before measurement for dissolved CO_2 (Figure 6a) and averaged over 15 days before the measurement for dissolved CH_4 (Figure 6b). However, an inspection of the distribution of residuals suggests that a linear regression was not the most appropriate model fit for dissolved CH_4 and that hysteresis loops were observed (Figure 6b).

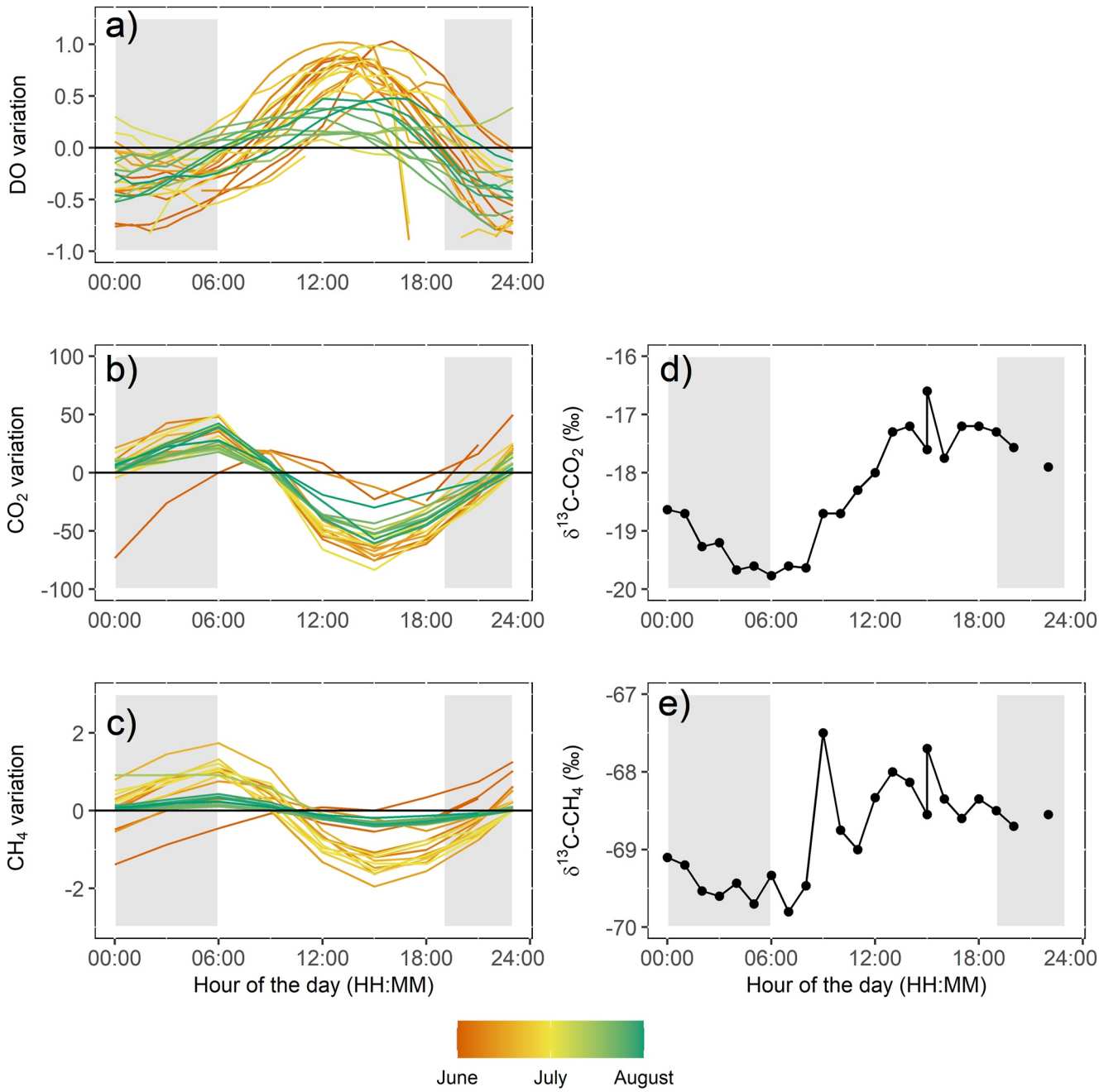

Figure 5. Diel variation of (a) dissolved oxygen (DO), (b) dissolved carbon dioxide (CO_2), (c) dissolved methane (CH_4) for the period 25 June to 18 August 2020; (d) $\delta^{13}C$-CO_2 and (e) $\delta^{13}C$-CH_4 for the period 1–2 August 2019 at the stream outlet (sampling point #8). For (a–c), the daily median value was subtracted from the hourly measured value. Days with >1 mm rain and the following 24 hr were removed to only compare variables' behavior during non-rain conditions. Gray background indicates nighttime.

3.2.4. Seasonal Estimates of CO_2 and CH_4 Losses (Emission and Downstream Export) at the Outlet

The 55-day time series presented in Figure 4 were used to calculate the downstream export and C-GHG emission at the seasonal scale. We applied an approach that accounted for the spatial variation of gases within the stream (see Equation 12 and Table S3 in Supporting Information S1). Results from this approach are presented in Figure 7.

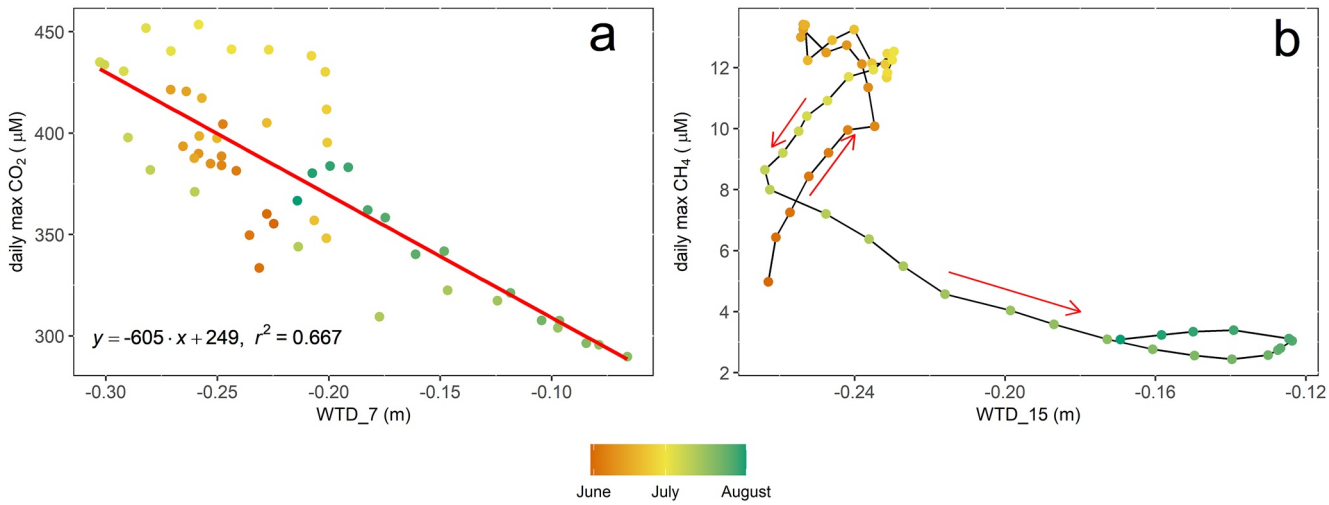

Figure 6. (a) Linear regression between dissolved carbon dioxide (CO_2) daily maximum values with peatland water table depth averaged over the 7 days before measurement and (b) plot of dissolved methane (CH_4) daily maximum value with peatland water table depth averaged over the 15 days before measurement. Note that all sampling days were considered here, including rainy days.

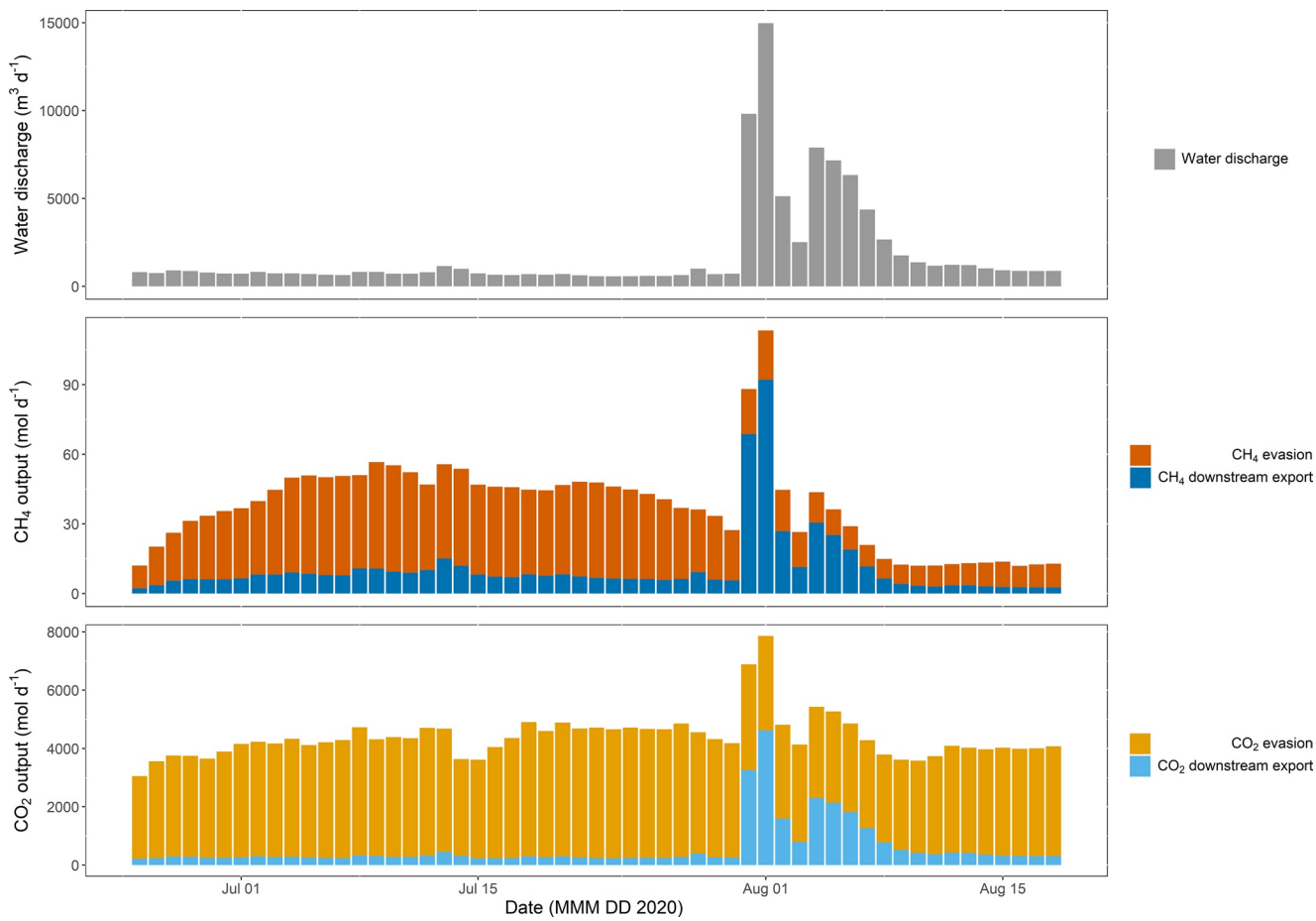

Figure 7. Time series of the daily water discharge, carbon dioxide (CO_2) and methane (CH_4) aquatic losses (cumulative atmospheric emission and downstream export) for the period 25 June–18 August 2020 based on continuous measurements at the outlet. A correction factor was applied to integrate longitudinal variation of CO_2 and CH_4 atmospheric emission along the stream (see Equations 11 and 12).

Over the full 55-day period, the largest aquatic C-GHG flux was CO_2 emission to the atmosphere (208.6 kmol) which accounted for 85.9% of total aquatic C-GHG losses (i.e., the sum of CO_2 + CH_4 emissions and CO_2 + CH_4 downstream export of 242.9 kmol). CO_2 downstream export was the second-largest flux (32.2 kmol) accounting for 13.3% of total aquatic C-GHG loss. CH_4 emissions (1.5 kmol) and CH_4 downstream export (0.6 kmol) represented the remaining 0.6% and 0.2% of the total aquatic C-GHG, respectively. When comparing losses to the atmosphere versus downstream export, 86.5% of the C-GHG was directly released to the atmosphere rather than exported downstream.

Over the time series, larger total carbon export (emission plus downstream export) was observed after rainy events. In particular, during events from 31 July to 1 August and from 4 to 5 August 2020 downstream export exceeded daily emission rates for both CO_2 and CH_4 (Figure 7). Those four days accounted for the largest daily losses of the time series (5,305–7,973 mol d^{-1}).

For the period from 25 June to 18 August 2020 (i.e., 55 days), a total of 2,918 kg C (or 2.47 g C m^{-2} when normalized over the catchment area of 1.18 km^2) was estimated to be lost from the stream (emissions + downstream export). If normalized over 180 days which was assumed to be the duration of the snow-free period in the region (Teodoru et al., 2009), our mass balance suggests that the peatland stream released 8.01 and 0.07 g C m^{-2} y^{-1} for CO_2 and CH_4, respectively.

3.2.5. Stormflow Versus Base Flow Analysis

Both dissolved CO_2 and CH_4 concentrations at the outlet had distinctive bimodal distributions that could be explained by the flow conditions. Lower concentrations were measured during the "stormflow" periods and higher concentrations were reported during the "base flow" (Figures 8a and 8b). Consequently, atmospheric flux emissions followed the same distribution (Figures 8c and 8d) since they were estimated based on concentrations and flow velocity. This was, nevertheless, not the case for downstream export (Figures 8e and 8f). Some rare but extremely strong fluxes occurred during stormflow events. For instance, the 10% peak downstream fluxes accounted for 46%, 42%, and 48% of the total, CH_4 and CO_2 downstream export, respectively. All those fluxes happened during the period from 31 July to 7 August when the highest rainfall events were recorded (Figure 4).

4. Discussion

The partial pressure of CO_2 and CH_4 along the stream (Figure 2) measured at our study site, with peatlands covering 64% of the catchment, was within the high range of other studies conducted on temperate and boreal streams (Table 1). The importance of surrounding terrestrial environments as drivers of stream functioning and fluvial carbon dynamics has gained recognition over the last decade (e.g., Campeau, Bishop, et al., 2017; Campeau, Wallin, et al., 2017; Crawford et al., 2013, 2014; Rasilo et al., 2017; Rocher-Ros et al., 2019). However, precise estimates of the contribution of porewater seepage in comparison to other sources are still limited (Hotchkiss et al., 2015). This study is an original contribution to estimate the respective contribution of CO_2 and CH_4 sources and estimate the total emissions from a peatland headwater stream.

4.1. Origins and Spatial Variations of CH_4 and CO_2 in a Peatland Headwater Stream

Stable isotopic values of CH_4 tend to support the hypothesis that CH_4 was laterally exported from peat porewater to the aquatic system. The δ^{13}C-CH_4 values measured in the peat porewater (−77.20 ± 3.58‰; Table S1 in Supporting Information S1) are typical for hydrogenotrophic methanogenesis (HM) commonly measured in northern peatlands (e.g., Conrad, 2005; Galand et al., 2010; Holmes et al., 2015). The δ^{13}C-CH_4 values measured in the stream (−60.94 ± 6.57‰) were comparable to peat porewater values, albeit heavier and more variable. Although the origin of CH_4 cannot be identified by stable isotopic signature alone, the closeness of δ^{13}C-CH_4 between the two systems (i.e., stream and peat porewater), the extremely high pCH_4 values measured in peat porewater (27,733 to 304,993 µatm) as well as its spatial variation with more depleted values when surrounded by peat only (e.g., sampling points #5 and #8; Figure 2d) support this argument. If not produced in the peat porewater, CH_4 could be produced in the hyporheic zone (riparian water-saturated zone) at the interface between the peatland and the stream. However, the CO_2:CH_4 ratio between the peat porewater (median = 8.4) and stream outlet (17; Table S1 in Supporting Information S1) shows a gain in CO_2 and/or loss of CH_4 concentrations in the stream. This suggests that CH_4 is likely to be oxidized and converted into CO_2 in the hyporheic zone, as previously

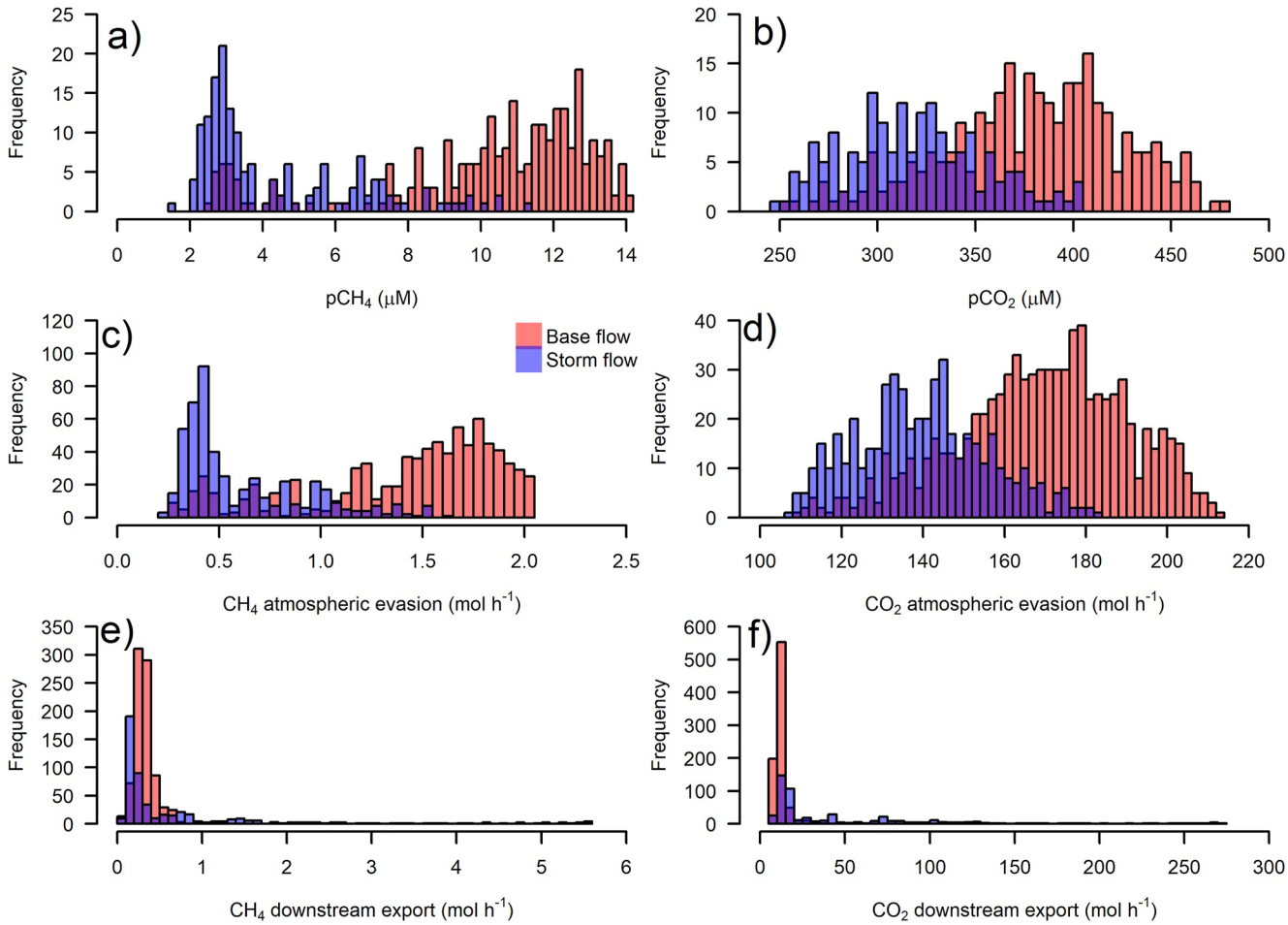

Figure 8. Frequency distribution of carbon dioxide (CO_2) and methane (CH_4) concentrations at the outlet station (a and b), atmospheric emission from the whole stream area (c and d), and downstream export from the outlet station (e and f). The hourly events were identified either as stormflow (blue bars), or base flow (red bars) based on their hourly discharge rate (see Section 2 for further details). Note the bimodal distribution for concentrations and emission as well as the nonnormal distribution for downstream export with few but strong events during storm flow.

reported by Rasilo et al. (2017), rather than newly produced. While CH_4 in the watershed seemed to be the product of peatland organic matter HM, CO_2 in the stream likely originated from multiple biogeochemical processes as suggested by the difference in δ^{13}C-CO_2 between peat porewater (mean = −4.18‰ (median = −3.8‰) ± −stdev = 2.83‰) and the stream (−20.76‰ (−20.60‰) ± 3.18‰; Table S1 in Supporting Information S1). Regarding peat porewater, the extremely enriched ^{13}C signature of dissolved CO_2 could result from the intense HM that appears to be occurring within the peat (based on the extremely high concentrations and depleted δ^{13}C signature of CH_4 observed in porewater). Indeed, HM strongly selects lighter CO_2 isotopes and generates highly enriched residual CO_2 (Okumura et al., 2016). The peat porewater value is substantially different from the soil porewater signature typically found in forested areas of around −30 ‰ to −25‰ as a result of C_3 organic matter respiration and degradation (Campeau, Bishop, et al., 2017; Campeau, Wallin, et al., 2017; Hutchins et al., 2020).

The supply of CO_2 in freshwater systems is the product of allochthonous and autochthonous processes. Allochthonous input can come from soil porewater lateral discharge (Öquist et al., 2009) or influx from the hyporheic zone (Rasilo et al., 2017). Since the mass balance model developed in this study was not able to differentiate those two processes, the term porewater seepage was used to qualify the allochthonous subsurface lateral input. Autochthonous CO_2 is the byproduct of in-stream productivity (which contains aquatic respiration (Hall et al., 2016) and photo-oxidation (Rocher-Ros et al., 2021)) and CO_2 release from methane oxidation. The mass balance developed in this study, based on concentrations, water discharge and flux data, provides an insight into

Journal of Geophysical Research: Biogeosciences
10.1029/2022JG006855

Table 1
Literature Review and Comparison of CO_2 and CH_4 Concentrations and Fluxes From Boreal and Temperate Streams

Study site	Stream order	Lat.	pCO_2 (µatm)	pCH_4 (µatm)	FCO_2 (mmol m^{-2} d^{-1})	FCH_4 (mmol m^{-2} d^{-1})	CO_2 catchment flux (gC m^{-2})	CH_4 catchment flux (gC m^{-2})	Reference
Peatland headwater stream (Quebec, Canada)	1	50.31	8,256 (8,093) ± 1,501 [2,044–23,306]	4,748 (5,253) ± 2,450 [14–17,614]	689 (689) ± 122 [146; 1,987]	5.28 (5.76) ± 3.36 [0.00; 46.32]	2.45 (55 days); 8.01 (180 days)	0.02 (55 days); 0.07 (180 days)	THIS STUDY
Boreal streams (Sweden)	1–4	68.2	[380; 3,400] ppm	NA	278–610 [0; 4,992]	NA	NA	NA	(Rocher-Ros et al., 2019)
Boreal streams (Sweden)	1–3?	68	3,990 ± 2,870 [460; 10,570]	880 ± 670 [100; 2,920]	1,299 (857)	15.84 (8.4)	8.6 ± 5.3 (130–135 days)	8.6 ± 5.3 (130–135 days)	(Lundin et al., 2013)
Thermokarst thaw-runoff streams (NWT, Canada)	1–3?	67.2	3,897 [658; 16,593]	83 [0; 1,357]	708 [43; 2,462];	0.0 [0.0; 2.4]	NA	NA	(Zolkos et al., 2019)
Boreal streams (Alaska, USA)	1–4	65.34	1,417 [570–2,600]	4	441	0.72	0.44 [0.08–1.22] (180 days)	NA	(Crawford et al., 2013)
Boreal streams (Sweden)	1–4	64.21	[722; 24,167]	[1,455; 6,411]	[331.; 1,459]		5.0 (365 days?)	NA	(M. B. Wallin et al., 2013)
Boreal streams (Finland)	??	61.04	NA	NA			7.0 ± 2.4 (??days)	0.1 ± 0.04 (??days)	(Huotari et al., 2013)
Peatland headwater stream (Scotland, UK)	1	56.93	[420; 4,500]	[0; 908]	[22; 3,821]	[0; 28.8]	14.1 (365 days)	0.1 (365 days)	(Hope et al., 2001)
Peatland headwater stream (Scotland, UK)	1	55.47	[906; 8,112]	25,418	5,798 ± 1,553	8.88 ± 1.92	14.02 (365 days)	0.003 (365 days)	(Dinsmore et al., 2010)
Peatland headwater streams (UK)	1–3	52–58	[671–10,271]	[1–7,518]	2,640 (958) [-43.2; 34,728]	10.32 (1.68) [10.8; 90.72]	NA	NA	(Billett & Harvey, 2013)
Boreal streams (Quebec, Canada)	1–5	51–52	243 [481–5,409]		259		NA	NA	(Teodoru et al., 2009)
Boreal streams (Quebec, Canada)	1–4	50–51	1,717 ± 139	1,111 ± 271	66 ± 7	1.92 ± 0.48	NA	NA	(Rasilo et al., 2017)
Boreal rivers and streams (Quebec, Canada)	1–6	47–49	2,959 [509–10,537]	1,781 [24–28,684]	74 [2–490]	8.16 [0–214.56]	1.04 (214 days)	1.04 (214 days)	(Campeau et al., 2014)
Temperate streams (Michigan, USA)	1	45.8	3,960 [40–12,040]	100	509 (490) [−50; 2,030]	8.4 [0; 0.12	3.74 (200 days)	3.74 (200 days)	(Crawford et al., 2014)
Temperate headwater stream (Ontario, Canada)	1	45.40	[3,850; 8,630]	[18; 160]	346 ± 266 [72; 991]	0.96 ± 0.48 [0.048; 1.92]	3.1 (250 days)	[0.012; 0.055]	(Billett & Moore, 2008)

Table 1
Continued

Study site	Stream order	Lat.	pCO_2 (µatm)	pCH_4 (µatm)	FCO_2 (mmol m^{-2} d^{-1})	FCH_4 (mmol m^{-2} d^{-1})	CO_2 catchment flux (gC m^{-2})	CH_4 catchment flux (gC m^{-2})	Reference
Temperate streams (Ontario, Canada)	1–2	45.19	[570; 23,500]		95 [49; 321]		NA	NA	(Koprivnjak et al., 2010)
Temperate streams (CT, USA)	1	41.43	3,534 (3,265) ± 1,419	315 (214) ± 297	569 (367) ± 636 [62; 5,515]	1.92 (1.44) ± 2.16 [0–14.64]	NA	NA	(K. S. Aho & Raymond, 2019)

Note. Data are presented in mean (median) ± standard deviation [min; max]; for catchment flux at our study site, data are presented as the range produced by our model when using the total watershed area and the peat covered watershed area; NA = data not available. Boreal stream refers to a drainage basin in the boreal zone that is not predominantly covered by peatlands. Temperate stream refers to a drainage basin in the temperate zone that is not predominantly covered by peatlands. Publications in this table present data related to low order stream and directly measured pCO_2 and pCH_4 on-site (i.e., regional estimates from upscaling and modeling were not considered). The sign "?" was used when the information was not explicitly given in the reference but deducted, when possible, or left blank.

the respective contribution of those sources and confirms our hypothesis that most CO_2 (88% of the total input) is from porewater seepage rather than in-stream processes (Figure 3).

Our mass balance model revealed that the lowest porewater seepage and associated downstream export (as opposed to in-stream CO_2 production) occurred in the most upstream segments *a* and *b* (Figure 3). Those two segments also had a depleted $\delta^{13}C\text{-}CO_2$ of about −25‰, close to what is expected for $\delta^{13}C$-DIC in a system where organic matter mineralization from heterotrophic bacteria respiration of C_3 vegetation is the driving process (Rocher-Ros et al., 2021; Waldron et al., 2007) but very far from the peat porewater $\delta^{13}C\text{-}CO_2$ value. Those two segments are located close to the edge of the peatland with coniferous and birch trees on the eastern side (Figure 1b). Thus, CO_2 at the head of the stream seemed to be dominated by lateral inputs of soil-derived CO_2, and in-stream mineralization of soils-derived organic matter rather than peat porewater seepage. As the stream flowed through the peat, pCO_2 values increased and so did the $\delta^{13}C\text{-}CO_2$ (Figures 2a and 2b), which is consistent with an increasing input of highly enriched $\delta^{13}C\text{-}CO_2$ likely originating in the peat porewater. The mass balance results suggest that porewater seepage and associated downstream export contributed at comparable proportions between the segments *c* to *g* (81%–93% of the total input; Figure 3). Segment *f* appeared to differ in behavior as compared to the other stream sections since a decrease of CO_2 load at the downstream point when compared to its upstream point (i.e., emission > input) was measured. This can be explained by high emission rates related to the high $k_{600\text{-}CO2}$ at this site (median = 3.6 m d^{-1}; Table S1 in Supporting Information S1) when compared to the other sections (k_{CO2} < 2.7 m d^{-1}) and the extensive stream surface area (1,603 m^2) when compared to the other sections (160–1,229 m^2).

On the other hand, an increase of both pCO_2 and pCH_4 observed along the stream between segments *f* and *g* (Figure 2) suggests that input was greater than the consumption from metabolic activity (for CO_2 only) and gas emission (for both CO_2 and CH_4), which was supported by our mass balance model (Figure 3). Headwater streams are considered to be hotspots for carbon emission because oversaturation leads to rapid and intense emissions toward the atmosphere (Rasilo et al., 2017). This is what has been observed in segments *c* to *f* (Figure 2). However, in two segments and despite high emission rates, porewater seepage input surpassed CO_2 and CH_4 losses (Figure 3). This was for example, the case in segment *g* where atmospheric emission was 375.9 mol d^{-1} while peat porewater seepage was 553.8 mol d^{-1}. This disproportionate porewater seepage contribution in segment *g* was further supported by the closer concentrations and stable isotopic values between point #8 ($\delta^{13}C\text{-}CO_2$ = −17.8‰) and peat porewater ($\delta^{13}C\text{-}CO_2$ = −3.8‰) when compared with the other sampling points ($\delta^{13}C\text{-}CO_2$ = −24.5 ‰ to −18‰; Table S1 in Supporting Information S1). Interestingly, DOC concentrations did not seem to follow the same trend (i.e., no abundant seepage of DOC) in segment *g* (Figure S5 in Supporting Information S1) even though peat porewater is a huge DOC reservoir. One explanation for the absence of consistency between the dissolved organic and inorganic carbon species is intense mineralization in the hyporheic zone, transforming organic carbon into CO_2 before being discharged into the stream (Fasching et al., 2014; Krause et al., 2011; Lapierre & Del Giorgio, 2014; Rasilo et al., 2017). One way to test this hypothesis would have been to collect DOC and pCO_2 samples in the hyporheic zone. Since $\delta^{13}C\text{-}CO_2$ in the peat porewater is very high (−3.80‰), an enriched $\delta^{13}C\text{-}CO_2$ in the hyporheic zone, closer to the $\delta^{13}C$-DOC values of −27.2‰ (Table S1 in Supporting Information S1), would have confirmed that DOC is mineralized in the hyporheic zone.

In summary, the combination of concentrations and stable isotopic values along the stream provides arguments to support that dissolved CO_2 and CH_4 originated predominantly from lateral porewater seepage and had been produced before being delivered to the stream. Moreover, the $\delta^{13}C\text{-}CO_2$ values suggested that the underlying processes shaping the riverine $\delta^{13}C\text{-}CO_2$ in this peat headwater stream are very different from what we see in other small order streams. The pattern of increasing $\delta^{13}C\text{-}CO_2$ along the riverine flow path reported in this study has been observed before (e.g., van Geldern et al., 2015). This increase generally occurs with a decline in pCO_2 and has been hypothesized to reflect the progressive degassing of oversaturated CO_2 from terrestrial origin in the headwaters (with a signature of around −26‰ or −27‰) and increasing mixing with atmospheric CO_2 which has a signature of around −8‰ (National Oceanic and Atmospheric Administration/Earth System Research Laboratory – Global Monitoring & Division, 2022). At our site, we see the pattern of increasing $\delta^{13}C\text{-}CO_2$ along the flow path,

but this is not accompanied by a systematic decline in pCO_2. Quite the opposite, local peaks of pCO_2 were measured downstream with, nevertheless, higher $\delta^{13}C\text{-}CO_2$ than upstream. Our interpretation is that the very upstream segments are completely dominated by inputs of terrestrial soil-derived CO_2 that has a $\delta^{13}C\text{-}CO_2$ signature between −25‰ and −27‰. As the stream flows through the peatland, this soil-derived CO_2 is emitted and is gradually replaced by peat-derived CO_2, which has a much higher $\delta^{13}C\text{-}CO_2$ value (somewhere between 0‰ and −10‰; Table S1 in Supporting Information S1). This would explain why the $\delta^{13}C\text{-}CO_2$ consistently increases along the flow path even though pCO_2 does not decline and in fact, at places, increases.

The pCH_4 and pCO_2 values measured along the stream were in the high range when compared to the literature (Table 1). Only studies also conducted in peatlands headwater streams reported such high values. This confirms our hypothesis that peatland ecosystems release a large amount of CH_4 and CO_2 through the aquatic pathway and must be accounted for to accurately estimate the carbon removal potential of peatlands specifically and wetlands in general (Taillardat et al., 2020; Webb et al., 2019). However, accurate estimates require integrating the spatial and temporal variability at the annual scale.

4.2. Processes and Key Variables Driving the Variation of Aquatic CO_2 and CH_4 Concentrations

Both CO_2 and CH_4 concentrations followed a diel pattern with greater concentrations at night and lower values during the day (Figure 5). For CO_2, it is explained by in-stream metabolism (e.g., Finlay, 2003; Rocher-Ros et al., 2020, 2021). Surprisingly, dissolved CH_4 also followed the same diel pattern as CO_2, with lower concentrations in the afternoon (Figure 5) but cannot be explained by in-stream metabolism. One possible explanation for this dissolved CH_4 diel pattern is that greater methanotrophic activity may be more important during the day because the temperature is higher (Mohanty et al., 2007). Despite noticeable changes, diel variations in CH_4 concentrations were rather limited when compared to the magnitude of CO_2 diel change (Figure 5b) and CH_4 seasonal concentration changes measured over the 55-day time series (Figure 4). This indicates that supply (i.e., porewater seepage) rather than in-stream transformation processes influence aquatic CH_4 concentrations and associated emissions or export. This is confirmed by our CH_4 mass balance model which shows that on average, CH_4 oxidation consumed less than 50% of the available CH_4 (Figure 3). Moreover, this may be an overestimation since our mass balance was based on daytime sample collection when methane oxidation may be greater as suggested above.

Previous studies have highlighted the strong hydrological and biogeochemical connectivity between low-order streams and their respective catchment (Crawford et al., 2014; Hotchkiss et al., 2015). Other studies shed light on the importance of wetlands to explain high dissolved carbon concentrations in streams when compared to other types of low order streams (Aho & Raymond, 2019; Dinsmore, Billett, et al., 2013; Dinsmore, Wallin, et al., 2013). However, lateral discharge dynamics and response to precipitation are not the same for all streams. At our site, we observed a negative relationship between CO_2 and CH_4 concentrations with water table depth (Figure 6) and discharge (Figure 8). Such negative relationships have been previously reported in peat headwater streams for CO_2 and CH_4 (Billett & Harvey, 2013; Dinsmore & Billett, 2008; Dinsmore et al., 2010; Dinsmore, Billett, et al., 2013; Dinsmore, Wallin, et al., 2013; Looman et al., 2017; Wallin et al., 2010). Conversely, a positive linear relationship between concentrations and water discharge has been reported from comparable low order streams covered with wetlands (Abril et al., 2014; Aho & Raymond, 2019; Crawford et al., 2013). One possible explanation is that a negative concentration-discharge relationship occurs in peatlands only. Peatlands are a specific wetland type with a deep organic porous peat layer able to hold large quantities of water. An interesting hydrological behavior of peatland headwater streams, also observed at our site, is that water is constantly flowing even during the driest periods because water stocks are important in comparison to other terrestrial ecosystems (Dinsmore, Billett, et al., 2013; Dinsmore, Wallin, et al., 2013). Nevertheless, a quick hydrological response to precipitation still happens (Dinsmore, Billett, et al., 2013; Dinsmore, Wallin, et al., 2013). Consequently, on the one hand, high CO_2 and CH_4 concentrations during baseflow periods are explained by constant peat porewater export. On the other hand, low CO_2 and CH_4 concentrations during stormflow periods can simply be explained by dilution and limited residence time. Wetlands with a thinner organic layer likely hold lower water and carbon stocks. Therefore, their hydrological behavior differs from peatlands. Such a difference would explain the divergent concentration-discharge relationships reported in the literature between peatland and non-peatland watersheds dominated streams.

The negative relationships between water table level with both CO_2 and CH_4 (Figure 6) indicate that deeper peat porewater—loaded with dissolved carbon—is exported during the dry period that followed a rain event. The effect of drought-induced lags in carbon loss from peatlands has been described before, using continuous eddy covariance time series (Brown et al., 2014; Goodrich et al., 2015). The rationale is that rising water table level prevents diffusive fluxes (Moore & Roulet, 1993) and rewet fresh labile organic carbon that can easily be decomposed in the following days (Knorr et al., 2009). First, through aerobic processes (i.e., producing CO_2) when the water table level remains close to the surface where O_2 is available. Second, through methanogenesis in deeper anoxic peat layers. The oxic/anoxic gradient throughout peat depth may explain why we observed a longer time lag for CH_4 concentrations when plotted against water table level (Figure 6). While the drought-induced lag effect was developed for carbon emissions at the peat-atmosphere interface, it seems to also apply to the lateral discharge of peat porewater to its drainage system. However, we note that in-stream CO_2 concentrations still remained high when CH_4 peaked (Figure 4). This can be explained by methane oxidation occurring along the lateral transfer from peat porewater to the stream, including in the hyporheic zone (see Section 4.1).

4.3. Implications of This Study for Constraining Global C-GHG Emissions and Determining the Importance of Aquatic Loss in a Peatland Net Ecosystem Carbon Budget

Combining longitudinal and spatial dissolved gas concentrations, water discharge, and flux data allowed us to derive a robust seasonal aquatic C-GHG budget for the entire stream section. While most of the longitudinal samplings were conducted during the low flow period (Figure S3 in Supporting Information S1), continuous measurements at the outlet allowed collecting data during stormflow periods (Figure 4). The 31 July to 10 August 2020 period represented 9 days within the 55 days of our continuous measurement data set but accounted for 61% and 50% of the CO_2 and CH_4 exported downstream, respectively (Figure 7). This was the result of intense rainfall, WTD rise and stream discharge. Similar results were presented by Dinsmore and Billett (2008) where 71% of the downstream export occurred during stormflow events. Thus, our results can relate to the "pulse-shunt concept" coined for organic matter dynamics in low order streams (Raymond et al., 2016) which appears to be also relevant to CO_2 and CH_4 export. The disproportionate contribution of short but intense hydrological events justifies the need to obtain long-term time series data sets integrating extreme events for accurate seasonal or annual carbon budget estimates. This is particularly important in the context of climate change where rain and storm events may increase in intensity, which could lead to an increase in aquatic-mediated peatland carbon losses.

Emission rates of CO_2 and CH_4 measured at our site were in the high range when compared with other studies (Table 1). For CO_2, two studies conducted in a Scottish stream surrounded by drained peatlands reported even higher fluxes, as high as 34.73 mol m^{-2} d^{-1} for CO_2 (Billett & Harvey, 2013; Dinsmore et al., 2010). This can be explained by the drainage effect that increased peat decomposition and potentially high stream turbulence, with flow rates as fast as 332 L s^{-1}. At our site, the maximum CO_2 emission was 1.99 mmol m^{-2} d^{-1} (Table 1) and water discharge never exceeded 55 L s^{-1}. For CH_4, the median (5,253 µatm; 8.76 µM) value measured was higher than in most high latitude low order streams (Table 1) but also when compared to a global data set (see Figure 3 in Stanley et al., 2016). However, the average CH_4 flux (5.28 mmol m^{-2} d^{-1}) did not exceed the range of the other reported studies (Table 1). Gas emission is the product of the water-air concentration gradient and gas exchange velocity. In peatland streams, water gas concentrations are high, but streams are usually slow-moving, which results in low gas exchange coefficients (Aho & Raymond, 2019). Thus, emissions appear to be energy-limited (i.e., low gas exchange) rather than supply limited. This is a fundamental difference with other headwater stream types such as mountain streams and any other high-channel slope streams (Aho & Raymond, 2019; Crawford et al., 2015; Ulseth et al., 2019) unless groundwater input is high (Horgby et al., 2019).

Our seasonal estimate suggests that 86.5% of the dissolved CO_2 and CH_4 present in the stream was emitted to the atmosphere within the catchment boundary rather than being exported downstream (Figure 7). Relatively slow flow rates provide sufficient time for the stream to degas to the atmosphere despite low gas exchange velocity. Moreover, the steady input of porewater seepage into the stream, as reported with our mass balance model (Figure 3), maintains oversaturation and continuous emission to the atmosphere. The catchment aquatic C-GHG budget for CO_2 and CH_4 suggests a seasonal loss of 2.47 g C m^{-2}, over a measurement period of 55 days. When adjusted to the whole year and the catchment scale, assuming a snow-free period of 180 days and no emission during the winter (frozen stream surface), the emissions are 8.08 g C m^{-2} y^{-1}. This estimate is within the high range when compared to other headwater streams CO_2 and CH_4 budgets from the boreal biome but similar to the

total aquatic carbon loss from studies in Scotland (Table 1). The greater aquatic C-GHG loss in the peatlands from Scotland is explained by the absence of snow cover and frozen streams which differs from North American boreal peatlands but, more importantly, by the fact that the study site is artificially drained (Billett & Harvey, 2013; Dinsmore et al., 2010). Although probably occurring at our site, winter CO_2 and CH_4 emissions and downstream export from the stream were not considered in this study. Similarly, the gas transfer velocities were developed during field visits that occurred mainly during baseflow periods. Thus, atmospheric emission during high flow velocity periods may have been underestimated as well. The annual budget of 8.08 g C m^{-2} y^{-1} is, therefore, a conservative estimate.

Our results suggest that about 81% of CO_2 present in the stream was from porewater lateral discharge while only 17% was from in-stream production and 2% from methane oxidation (Figure 3). These proportions are close to the 90% contribution of soil water estimated from the first-order stream by Butman and Raymond (2011) and the median of 14% (range: 0%–19%) from aquatic metabolism reported by Hotchkiss et al. (2015) in low discharge streams. Therefore, our study is an additional contribution to support that peatlands sustain high dissolved C-GHG during both base flow and stormflow periods. However, the atmospheric fluxes of C-GHG were not highest in our studied stream when compared to others, despite the high C-GHG concentrations reported (Table 1) which were explained by the low gas transfer velocities. Nevertheless, it is likely that most of the peat-derived dissolved CO_2 and CH_4 exported downstream will ultimately evade to the atmosphere along the aquatic continuum (Aho & Raymond, 2019) and should therefore be accounted for as a net loss in a net ecosystem carbon budget.

Primeau and Garneau (2021) estimated a long-term (i.e., Holocene) apparent rate of carbon accumulation (LORCA) of 35.5 g C m^{-2} y^{-1} and a recent apparent rate of carbon accumulation (RERCA) of 86.1 g C m^{-2} y^{-1} for the period 1965–2016 at our site. Applying a correction from those carbon sequestration rates to integrate aquatic C-GHG loss reported in this study would require dating the carbon being released, which was not measured in this study. Thus, our study alone does not allow us to close the net ecosystem carbon budget because no site-specific radiocarbon dating was conducted and other carbon outputs from the ecosystem budget will need to be quantified. Still, this study demonstrates that streams flowing through peatlands act as a large C-GHG source that needs to be considered for complete net ecosystem carbon budget estimates.

5. Conclusion

This study contributes to further advancing biogeochemical concepts but also shows that peatland headwater streams have specificities when compared to other types of headwater streams for at least three reasons. First, enriched $\delta^{13}C\text{-}CO_2$ and depleted $\delta^{13}C\text{-}CH_4$ in both the peat porewater and stream suggest that hydrogenotrophic methanogenesis is an important source of CO_2 and CH_4 in a peatland dominated watershed as opposed to forest-dominated catchments. This specificity leads to a unique $\delta^{13}C\text{-}CO_2$ behavior along the stream with depletion of $\delta^{13}C\text{-}CO_2$ toward downstream but, in places, a gain of pCO_2 due to the peat porewater discharge. Second, the negative relationship between discharge and C-GHG concentrations is opposite to what has been reported in other wetland types. Our interpretation is that the water and carbon stocks in peat layers are so important that, even during low flow periods, a steady lateral flux of peat-derived carbon is laterally discharged to the stream. Third, dissolved C-GHG concentrations in peat streams are higher than in other types of headwater streams. Nevertheless, the total C-GHG loss appears to be equivalent to what is reported from most headwater streams but can increase by 15% if we include the downstream export which is likely to be ultimately released to the atmosphere farther down the stream network.

The aquatic CO_2 and CH_4 dynamics description and budget quantification presented in this study highlight the importance of integrating spatial and temporal measurements to comprehensively characterize stream functioning. Furthermore, the combination of downstream export and surface water emission is the only way to accurately estimate the stream-generated C-GHG loss. The combination of a mass balance based on spatiotemporal measurements and a 55-day detailed C-GHG budget enabled us to evidence that most C-GHG in this peatland headwater stream is from peat porewater discharge and released to the atmosphere rather than being laterally exported. We also showed that storm events substantially influence the total C-GHG budget since 46% of the total C-GHG loss occurred within 10% of the measurement time. The disparity in C-GHG emissions along the stream and fluctuation of downstream export over time has important implications for carbon flux estimates and predictions based on climate scenarios. Thus, the development of systematic surveys that integrates the spatial

and temporal variability is necessary to constrain the contribution of headwater catchments to the regional and global carbon budget.

Conflict of Interest

The authors declare no conflicts of interest relevant to this study.

Data Availability Statement

Data and metadata are available in the international research data repository Zenodo at (https://doi.org/10.5281/zenodo.6073957).

Acknowledgments
This research was funded by the Natural Sciences and Engineering Research Council of Canada and Hydro-Quebec to Michelle Garneau (RDCPJ 514218–17). The authors would like to thank Frederic Guérin for preliminary discussions on dissolved gas sampling and analysis, Katherine Velghe for laboratory training and assistance, Paul Baudron for access to his laboratory for radium analysis, the Geo-Lab at the National University of Singapore Department of Geography for using the the RAD7 Radon Detector, Cynthia Soued for her support for the metabolism calculations, Judith Rosentreter for her advice on aquatic flux measurements and local gas transfer velocity determination, as well as Charles Bonneau, Pénélope Germain-Chartrand, Charles-Élie Dubé-Poirier, Camille Girard, Léonie Perrier, Guillaume Primeau, Roman Teisserenc, and Karelle Trottier for their assistance in the field. The constructive comments made by Diego Riveros-Iregui, one anonymous reviewer, and the editors are gratefully acknowledged.

References

Abril, G., Martinez, J. M., Artigas, L. F., Moreira-Turcq, P., Benedetti, M. F., Vidal, L., et al. (2014). Amazon River carbon dioxide outgassing fuelled by wetlands. *Nature*, *505*(7483), 395–398. https://doi.org/10.1038/nature12797

Aho, K. S., Fair, J. H., Hosen, J. D., Kyzivat, E. D., Logozzo, L. A., Rocher-Ros, G., et al. (2021). Distinct concentration-discharge dynamics in temperate streams and rivers: CO_2 exhibits chemostasis while CH_4 exhibits source limitation due to temperature control. *Limnology & Oceanography*, *66*(10), 3656–3668. https://doi.org/10.1002/lno.11906

Aho, K. S., & Raymond, P. A. (2019). Differential response of greenhouse gas evasion to storms in forested and wetland streams. *Journal of Geophysical Research: Biogeosciences*, *124*(3), 649–662. https://doi.org/10.1029/2018JG004750

Appling, A. P., Hall, R. O., Yackulic, C. B., & Arroita, M. (2018). Overcoming equifinality: Leveraging long time series for stream metabolism estimation. *Journal of Geophysical Research: Biogeosciences*, *123*(2), 624–645. https://doi.org/10.1002/2017JG004140

Appling, A. P., Read, J. S., Winslow, L. A., Arroita, M., Bernhardt, E. S., Griffiths, N. A., et al. (2018). Data descriptor: The metabolic regimes of 356 rivers in the United States. *Scientific Data*, *5*, 1–14. https://doi.org/10.1038/sdata.2018.292

Attermeyer, K., Casas-Ruiz, J. P., Fuss, T., Pastor, A., Cauvy-Fraunié, S., Sheath, D., et al. (2021). Carbon dioxide fluxes increase from day to night across European streams. *Communications Earth & Environment*, *2*(1), 1–8. https://doi.org/10.1038/s43247-021-00192-w

Aufdenkampe, A. K., Mayorga, E., Raymond, P. A., Melack, J. M., Doney, S. C., Alin, S. R., et al. (2011). Riverine coupling of biogeochemical cycles between land, oceans, and atmosphere. *Frontiers in Ecology and the Environment*, *9*(1), 53–60. https://doi.org/10.1890/100014

Battin, T. J., Kaplan, L. A., Findlay, S., Hopkinson, C. S., Marti, E., Packman, A. I., et al. (2009). Biophysical controls on organic carbon fluxes in fluvial networks. *Nature Geoscience*, *2*(8), 595. https://doi.org/10.1038/ngeo602

Billett, M. F., & Harvey, F. H. (2013). Measurements of CO_2 and CH_4 evasion from UK peatland headwater streams. *Biogeochemistry*, *114*(1–3), 165–181. https://doi.org/10.1007/s10533-012-9798-9

Billett, M. F., & Moore, T. R. (2008). Supersaturation and evasion of CO2 and. CH4 in surface waters at Mer Bleue peatland (Vol. *2054*, pp. 2044–2054). https://doi.org/10.1002/hyp

Borges, A. V., Darchambeau, F., Lambert, T., Morana, C., Allen, G. H., Tambwe, E., et al. (2019). Variations in dissolved greenhouse gases (CO_2, CH_4, N_2O) in the Congo River network overwhelmingly driven by fluvial-wetland connectivity. *Biogeosciences*, *16*(19), 3801–3834. https://doi.org/10.5194/bg-16-3801-2019

Brown, M., Humphreys, E. R., Moore, T. R., Roulet, N. T., & Lafleur, P. (2014). Evidence for a nonmonotonic relationship between ecosystem-scale peatland methane emissions and water table depth. *Journal of Geophysical Research: Biogeosciences*, *119*, 2292–2311. https://doi.org/10.1002/2013JG002576.Received

Butman, D., & Raymond, P. A. (2011). Significant efflux of carbon dioxide from streams and rivers in the United States. *Nature Geoscience*, *4*(12), 839–842. https://doi.org/10.1038/ngeo1294

Butman, D., Stackpoole, S., Stets, E., McDonald, C. P., Clow, D. W., & Striegl, R. G. (2016). Aquatic carbon cycling in the conterminous United States and implications for terrestrial carbon accounting. *Proceedings of the National Academy of Sciences of the United States of America*, *113*(1), 58–63. https://doi.org/10.1073/pnas.1512651112

Campeau, A., Bishop, K., Amvrosiadi, N., Billett, M. F., Garnett, M. H., Laudon, H., et al. (2019). Current forest carbon fixation fuels stream CO_2 emissions. *Nature Communications*, *10*(1), 1–9. https://doi.org/10.1038/s41467-019-09922-3

Campeau, A., Bishop, K., Nilsson, M. B., Klemedtsson, L., Laudon, H., Leith, F. I., et al. (2018). Stable carbon isotopes reveal soil-stream DIC linkages in contrasting headwater catchments. *Journal of Geophysical Research: Biogeosciences*, *123*(1), 149–167. https://doi.org/10.1002/2017JG004083

Campeau, A., Bishop, K. H., Billett, M. F., Garnett, M. H., Laudon, H., Leach, J. A., et al. (2017). Aquatic export of young dissolved and gaseous carbon from a pristine boreal fen: Implications for peat carbon stock stability. *Global Change Biology*, *23*(12), 5523–5536. https://doi.org/10.1111/gcb.13815

Campeau, A., Lapierre, J., Vachon, D., & Del Giorgio, P. A. (2014). Global biogeochemical cycles boreal landscape of Québec. *Global Biogeochemical Cycles*. (1), 57–69. https://doi.org/10.1002/2013GB004685.Received

Campeau, A., Wallin, M. B., Giesler, R., Löfgren, S., Mörth, C. M., Schiff, S., et al. (2017). Multiple sources and sinks of dissolved inorganic carbon across Swedish streams, refocusing the lens of stable C isotopes. *Scientific Reports*, *7*(1), 1–14. https://doi.org/10.1038/s41598-017-09049-9

Clow, D. W., Striegl, R. G., & Dornblaser, M. M. (2021). Spatiotemporal dynamics of CO_2 gas exchange from headwater mountain streams. *Journal of Geophysical Research: Biogeosciences*, *126*(9), 1–18. https://doi.org/10.1029/2021JG006509

Cole, J. J., Prairie, Y. T., Caraco, N. F., McDowell, W. H., Tranvik, L. J., Striegl, R. G., et al. (2007). Plumbing the global carbon cycle: Integrating inland waters into the terrestrial carbon budget. *Ecosystems*, *10*(1), 171–184. https://doi.org/10.1007/s10021-006-9013-8

Conrad, R. (2005). Quantification of methanogenic pathways using stable carbon isotopic signatures: A review and a proposal. *Organic Geochemistry*, *36*(5), 739–752. https://doi.org/10.1016/j.orggeochem.2004.09.006

Core Team, R. (2021). A language and environment for statistical computing. Retrieved from https://www.r-project.org/

Crawford, J. T., Dornblaser, M. M., Stanley, E. H., Clow, D. W., & Striegl, R. G. (2015). Source limitation of carbon gas emissions in high-elevation mountain streams and lakes. *Journal of Geophysical Research: Biogeosciences*, *120*, 707–723. https://doi.org/10.1002/2014JG002861. Received

Crawford, J. T., Lottig, N. R., Stanley, E. H., Walker, J. F., Hanson, P. C., Finlay, J. C., & Striegl, R. G. (2014). CO_2 and CH_4 emissions from streams in a lake-rich landscape: Patterns, controls, and regional significance. *Global Biogeochemical Cycles*, (3), 197–210. https://doi.org/10.1111/1462-2920.13280

Crawford, J. T., Striegl, R. G., Wickland, K. P., Dornblaser, M. M., & Stanley, E. H. (2013). Emissions of carbon dioxide and methane from a headwater stream network of interior Alaska. *Journal of Geophysical Research: Biogeosciences*, *118*(2), 482–494. https://doi.org/10.1002/jgrg.20034

Dawson, J. J. C., Billett, M. F., Hope, D., Palmer, S. M., & Deacon, C. M. (2004). Sources and sinks of aquatic carbon in a peatland stream continuum. *Biogeochemistry*, *70*(1), 71–92. https://doi.org/10.1023/B:BIOG.0000049337.66150.f1

Dinsmore, K. J., & Billett, M. F. (2008). Continuous measurement and modeling of CO_2 losses from a peatland stream during stormflow events. *Water Resources Research*, *44*(12), 1–11. https://doi.org/10.1029/2008WR007284

Dinsmore, K. J., Billett, M. F., & Dyson, K. E. (2013). Temperature and precipitation drive temporal variability in aquatic carbon and GHG concentrations and fluxes in a peatland catchment. *Global Change Biology*, *19*(7), 2133–2148. https://doi.org/10.1111/gcb.12209

Dinsmore, K. J., Billett, M. F., Skiba, U. M., Rees, R. M., Drewer, J., & Helfter, C. (2010). Role of the aquatic pathway in the carbon and greenhouse gas budgets of a peatland catchment. *Global Change Biology*, *16*(10), 2750–2762. https://doi.org/10.1111/j.1365-2486.2009.02119.x

Dinsmore, K. J., Wallin, M. B., Johnson, M. S., Billett, M. F., Bishop, K., Pumpanen, J., & Ojala, A. (2013). Contrasting CO_2 concentration discharge dynamics in headwater streams: A multi-catchment comparison. *Journal of Geophysical Research: Biogeosciences*, *118*(2), 445–461. https://doi.org/10.1002/jgrg.20047

Downing, J. A., Cole, J. J., Duarte, C. M., Middelburg, J. J., Melack, J. M., Prairie, Y. T., et al. (2012). Global abundance and size distribution of streams and rivers. *Inland Waters*, *2*(4), 229–236. https://doi.org/10.5268/IW-2.4.502

Duvert, C., Butman, D. E., Marx, A., Ribolzi, O., & Hutley, L. B. (2018). CO_2 evasion along streams driven by groundwater inputs and geomorphic controls. *Nature Geoscience*, *11*(11), 813–818. https://doi.org/10.1038/s41561-018-0245-y

Fasching, C., Behounek, B., Singer, G. A., & Battin, T. J. (2014). Microbial degradation of terrigenous dissolved organic matter and potential consequences for carbon cycling in brown-water streams. *Scientific Reports*, *4*, 1–7. https://doi.org/10.1038/srep04981

Finlay, J. C. (2003). Controls of streamwater dissolved inorganic carbon dynamics in a forested watershed. *Biogeochemistry*, *62*(3), 231–252. https://doi.org/10.1023/A:1021183023963

Galand, P. E., Yrjäla, K., & Conrad, R. (2010). Stable carbon isotope fractionation during methanogenesis in three boreal peatland ecosystems. *Biogeosciences*, *7*(11), 3893–3900. https://doi.org/10.5194/bg-7-3893-2010

Goldenfum, J. A. (2010). GHG measurement guidelines for freshwater reservoirs.

Goodrich, J. P., Campbell, D. I., Roulet, N. T., Clearwater, M. J., & Schipper, L. A. (2015). Overriding control of methane flux temporal variability by water table dynamics in a Southern Hemisphere, raised bog. *Journal of Geophysical Research: Biogeosciences*, *120*, 707–723. https://doi.org/10.1002/2014JG002844.Received

Granéli, W., Lindell, M., De Faria, B. M., & Esteves, F. D. A. (1998). Photoproduction of dissolved inorganic carbon in temperate and tropical lakes - Dependence on wavelength band and dissolved organic carbon concentration. *Biogeochemistry*, *43*(2), 175–195. https://doi.org/10.1023/A:1006042629565

Guérin, F., & Abril, G. (2007). Significance of pelagic aerobic methane oxidation in the methane and carbon budget of a tropical reservoir. *Journal of Geophysical Research*, *112*(3), 1–14. https://doi.org/10.1029/2006JG000393

Hall, R. O., Jr., & Hotchkiss, E. R. (2017). Stream metabolism. In G. A. Lamberti & F. R. Hauer (Eds.), *Methods in stream ecology* (3rd ed., pp. 219–233). Academic Press. chap. 34.

Hall, R. O., & Madinger, H. L. (2018). Use of argon to measure gas exchange in turbulent mountain streams. *Biogeosciences*, *15*(10), 3085–3092. https://doi.org/10.5194/bg-15-3085-2018

Hall, R. O., Tank, J. L., Baker, M. A., Rosi-Marshall, E. J., & Hotchkiss, E. R. (2016). Metabolism, gas exchange, and carbon spiraling in rivers. *Ecosystems*, *19*(1), 73–86. https://doi.org/10.1007/s10021-015-9918-1

Hanson, R. S., & Hanson, T. (1996). Methanotrophic bacteria. *Microbiological Reviews*, *60*(2), 439471.

Holmes, M. E., Chanton, J. P., Tfaily, M. M., & Orgam, A. (2015). CO_2 and CH_4 isotope compositions and production pathways in a tropical peatland. *Global Biogeochemical Cycles*, *29*, 1–18. https://doi.org/10.1111/1462-2920.13280

Hope, D., Palmer, S. M., Billett, M. F., & Dawson, J. J. C. (2001). Carbon dioxide and methane evasion from a temperate peatland stream. *Limnology & Oceanography*, *46*(4), 847–857. https://doi.org/10.4319/lo.2001.46.4.0847

Horgby, Å., Boix Canadell, M., Ulseth, A. J., Vennemann, T. W., & Battin, T. J. (2019). High-resolution spatial sampling identifies groundwater as driver of CO_2 dynamics in an alpine stream network. *Journal of Geophysical Research: Biogeosciences*, *124*(7), 1961–1976. https://doi.org/10.1029/2019JG005047

Hotchkiss, E. R., Hall, R. O., Sponseller, R. A., Butman, D., Klaminder, J., Laudon, H., et al. (2015). Sources of and processes controlling CO_2 emissions change with the size of streams and rivers. *Nature Geoscience*, *8*(9), 696–699. https://doi.org/10.1038/ngeo2507

Huotari, J., Nykänen, H., Forsius, M., & Arvola, L. (2013). Effect of catchment characteristics on aquatic carbon export from a boreal catchment and its importance in regional carbon cycling. *Global Change Biology*, *19*(12), 3607–3620. https://doi.org/10.1111/gcb.12333

Hutchins, R. H. S., Tank, S. E., Olefeldt, D., Quinton, W. L., Spence, C., Dion, N., et al. (2020). Fluvial CO_2 and CH_4 patterns across wildfire-disturbed ecozones of subarctic Canada: Current status and implications for future change. *Global Change Biology*, *26*(4), 2304–2319. https://doi.org/10.1111/gcb.14960

Knorr, K. H., Lischeid, G., & Blodau, C. (2009). Dynamics of redox processes in a minerotrophic fen exposed to a water table manipulation. *Geoderma*, *153*(3–4), 379–392. https://doi.org/10.1016/j.geoderma.2009.08.023

Koprivnjak, J. F., Dillon, P. J., & Molot, L. A. (2010). Importance of CO_2 evasion from small boreal streams. *Global Biogeochemical Cycles*, *24*, 1–9. https://doi.org/10.1029/2009GB003723

Krause, S., Hanah, D. M., Fleckenstein, C., Heppell, C. M., Kaeser, D., Pickup, R., et al. (2011). Inter-disciplinary perspectives on processes in the hyporheic zone. *Ecohydrology*, *4*, 481–499. https://doi.org/10.1002/eco

Lapierre, J. F., & Del Giorgio, P. A. (2014). Partial coupling and differential regulation of biologically and photochemically labile dissolved organic carbon across boreal aquatic networks. *Biogeosciences*, *11*(20), 5969–5985. https://doi.org/10.5194/bg-11-5969-2014

Lide, D. R. (2007). *Handbook of chemistry and physics* (88th ed.). CRC Press.

Looman, A., Maher, D. T., Pendall, E., Bass, A., & Santos, I. R. (2017). The carbon dioxide evasion cycle of an intermittent first- order stream: Contrasting water – Air and soil – Air exchange. *Biogeochemistry*, *132*, 87–102. https://doi.org/10.1007/s10533-016-0289-2

Lorke, A., Bodmer, P., Noss, C., Alshboul, Z., Koschorreck, M., Somlai-Haase, C., et al. (2015). Technical note: Drifting versus anchored flux chambers for measuring greenhouse gas emissions from running waters. *Biogeosciences*, *12*(23), 7013–7024. https://doi.org/10.5194/bg-12-7013-2015

Lundin, E. J., Giesler, R., Persson, A., Thompson, M. S., & Karlsson, J. (2013). Integrating carbon emissions from lakes and streams in a subarctic catchment. *Journal of Geophysical Research: Biogeosciences*, *118*(3), 1200–1207. https://doi.org/10.1002/jgrg.20092

MacIntyre, S., Wanninkhof, R., & Chanton, J. P. (1995). Trace gas exchange across the air-water interface in freshwaters and coastal marine environments. In *Biogenic trace gasses: Measuring emis ions from soils and waters* (pp. 52–57). Blackwell.

Mannich, M., Fernandes, C. V. S., & Bleninger, T. B. (2019). Uncertainty analysis of gas flux measurements at air–water interface using floating chambers. *Ecohydrology and Hydrobiology*, *19*(4), 475–486. https://doi.org/10.1016/j.ecohyd.2017.09.002

Marx, A., Dusek, J., Jankovec, J., Sanda, M., Vogel, T., van Geldern, R., et al. (2017). A review of CO_2 and associated carbon dynamics in headwater streams: A global perspective. *Reviews of Geophysics*, *55*(2), 560–585. https://doi.org/10.1002/2016RG000547

Mohanty, S. R., Bodelier, P. L. E., & Conrad, R. (2007). Effect of temperature on composition of the methanotrophic community in rice field and forest soil. *FEMS Microbiology Ecology*, *62*(1), 24–31. https://doi.org/10.1111/j.1574-6941.2007.00370.x

Moore, T. R., & Roulet, N. T. (1993). Methane flux: Water table relations in northern wetlands. *Geophysical Research Letters*, *20*(7), 587–590. https://doi.org/10.1029/93GL00208

Moustapha, M., Deirmendjian, L., Sebag, D., Braun, J. J., Audry, S., Ateba Bessa, H., et al. (2022). Partitioning carbon sources between wetland and well-drained ecosystems to a tropical first-order stream - Implications for carbon cycling at the watershed scale (Nyong, Cameroon). *Biogeosciences*, *19*(1), 137–163. https://doi.org/10.5194/bg-19-137-2022

National Oceanic and Atmospheric Administration / Earth System Research Laboratory – Global Monitoring & Division. (2022). ESRL/GML. Retrieved from https://gml.noaa.gov/outreach/isotopes/c13tellsus.html

Okumura, T., Kawagucci, S., Saito, Y., Matsui, Y., Takai, K., & Imachi, H. (2016). Hydrogen and carbon isotope systematics in hydrogenotrophic methanogenesis under H2-limited and H2-enriched conditions: Implications for the origin of methane and its isotopic diagnosis. *Progress in Earth and Planetary Science*, *3*(1), 2–15. https://doi.org/10.1186/s40645-016-0088-3

Öquist, M. G., Wallin, M., Seibert, J., Bishop, K., & Laudon, H. (2009). Dissolved inorganic carbon export across the soil/stream interface and its fate in a boreal headwater stream. *Environmental Science and Technology*, *43*(19), 7364–7369. https://doi.org/10.1021/es900416h

Payette, S., Mortin, M. J., & Gamache, I. (2001). The subarctic forest-tundra: The structure of a biome in a changing landscape. *BioScience*, *51*, 709–718. https://doi.org/10.1641/0006-3568(2001)051[0709:tsftts]2.0.co;2

Picarro Inc. (2016). Picarro g2201-i analyzer data sheet.

Primeau, G., & Garneau, M. (2021). Carbon accumulation in peatlands along a boreal to subarctic transect in eastern Canada. *The Holocene*, (1), 1–12. https://doi.org/10.1177/0959683620988031

Rasilo, T., Hutchins, R. H. S., Ruiz-González, C., & del Giorgio, P. A. (2017). Transport and transformation of soil-derived CO_2, CH_4 and DOC sustain CO_2 supersaturation in small boreal streams. *Science of the Total Environment*, *579*, 902–912. https://doi.org/10.1016/j.scitotenv.2016.10.187

Raymond, P. A., Saiers, J. E., & Sobczak, W. V. (2016). Hydrological and biogeochemical controls on watershed dissolved organic matter transport: Pulse-shunt concept. *Ecology*, *97*(1), 5–16.

Rocher-Ros, G., Harms, T. K., Sponseller, R. A., Väisänen, M., Mörth, C. M., & Giesler, R. (2021). Metabolism overrides photo-oxidation in CO_2 dynamics of Arctic permafrost streams. *Limnology & Oceanography*, *66*(S1), S169–S181. https://doi.org/10.1002/lno.11564

Rocher-Ros, G., Sponseller, R. A., Bergström, A. K., Myrstener, M., & Giesler, R. (2020). Stream metabolism controls diel patterns and evasion of CO_2 in Arctic streams. *Global Change Biology*, *26*(3), 1400–1413. https://doi.org/10.1111/gcb.14895

Rocher-Ros, G., Sponseller, R. A., Lidberg, W., Mörth, C., & Giesler, R. (2019). Landscape process domains drive patterns of CO_2 evasion from river networks. *Limnology and Oceanography Letters*, *4*(4), 87–95. https://doi.org/10.1002/lol2.10108

Rosentreter, J. A., Borges, A. V., Deemer, B. R., Holgerson, M. A., Liu, S., Song, C., et al. (2021). Half of global methane emissions come from highly variable aquatic ecosystem sources. *Nature Geoscience*, *14*(4), 225–230. https://doi.org/10.1038/s41561-021-00715-2

Rosentreter, J. A., Maher, D. T., Ho, D. T., Call, M., Barr, J. G., & Eyre, B. D. (2017). Spatial and temporal variability of CO_2 and CH_4 gas transfer velocities and quantification of the CH_4 microbubble flux in mangrove dominated estuaries. *Limnology & Oceanography*, *62*(2), 561–578. https://doi.org/10.1002/lno.10444

Schelker, J., Singer, G. A., Ulseth, A. J., Hengsberger, S., & Battin, T. J. (2016). CO_2 evasion from a steep, high gradient stream network: Importance of seasonal and diurnal variation in aquatic pCO_2 and gas transfer. *Limnology & Oceanography*, *61*(5), 1826–1838. https://doi.org/10.1002/lno.10339

Schneider, C. L., Herrera, M., Raisle, M. L., Murray, A. R., Whitmore, K. M., Encalada, A. C., et al. (2020). Carbon dioxide (CO_2) fluxes from terrestrial and aquatic environments in a high-altitude tropical catchment. *Journal of Geophysical Research: Biogeosciences*, *125*(8), 1–13. https://doi.org/10.1029/2020JG005844

Schubert, C. J., Vazquez, F., Lösekann-Behrens, T., Knittel, K., Tonolla, M., & Boetius, A. (2011). Evidence for anaerobic oxidation of methane in sediments of a freshwater system (Lago di Cadagno). *FEMS Microbiology Ecology*, *76*(1), 26–38. https://doi.org/10.1111/j.1574-6941.2010.01036.x

Shelley, F., Abdullahi, F., Grey, J., & Trimmer, M. (2015). Microbial methane cycling in the bed of a chalk river: Oxidation has the potential to match methanogenesis enhanced by warming. *Freshwater Biology*, *60*(1), 150–160. https://doi.org/10.1111/fwb.12480

Shen, J. (1981). Discharge characteristics of triangular-notch thin-plate weirs.

Sivan, O., Adler, M., Pearson, A., Gelman, F., Bar-Or, I., John, S. G., & Eckert, W. (2011). Geochemical evidence for iron-mediated anaerobic oxidation of methane. *Limnology & Oceanography*, *56*(4), 1536–1544. https://doi.org/10.4319/lo.2011.56.4.1536

Stanley, E. H., Casson, N. J., Christel, S. T., Crawford, J. T., Loken, L. C., & Oliver, S. K. (2016). The ecology of methane in streams and rivers: Patterns, controls, and global significance. *Ecological Monographs*, *86*(2), 146–171. https://doi.org/10.1890/15-1027

Taillardat, P., Thompson, B. S., Garneau, M., Trottier, K., & Friess, D. A. (2020). Climate change mitigation potential of wetlands and the cost-effectiveness of their restoration. *Interface Focus*, *10*(5), 20190129. https://doi.org/10.1098/rsfs.2019.0129

Taillardat, P., Willemsen, P., Marchand, C., Friess, D. A., Widory, D., Baudron, P., et al. (2018). Assessing the contribution of porewater discharge in carbon export and CO_2 evasion in a mangrove tidal creek (Can Gio, Vietnam). *Journal of Hydrology*, *563*, 303–318. https://doi.org/10.1016/j.jhydrol.2018.05.042

Teodoru, C. R., Del Giorgio, P. A., Prairie, Y. T., & Camire, M. (2009). Patterns in pCO_2 in boreal streams and rivers of northern Quebec, Canada. *Global Biogeochemical Cycles*, *23*(2), 1–11. https://doi.org/10.1029/2008GB003404

Thottathil, S. D., Reis, P. C. J., del Giorgio, P. A., & Prairie, Y. T. (2018). The extent and regulation of summer methane oxidation in northern lakes. *Journal of Geophysical Research: Biogeosciences*, *123*(10), 3216–3230. https://doi.org/10.1029/2018JG004464

Tunaley, C., Tetzlaff, D., Wang, H., & Soulsby, C. (2018). Spatio-temporal diel DOC cycles in a wet, low energy, northern catchment: Highlighting and questioning the sub-daily rhythms of catchment functioning. *Journal of Hydrology*, *563*, 962–974. https://doi.org/10.1016/j.jhydrol.2018.06.056

Ulseth, A. J., Hall, R. O., Boix Canadell, M., Madinger, H. L., Niayifar, A., & Battin, T. J. (2019). Distinct air–water gas exchange regimes in low- and high-energy streams. *Nature Geoscience*, *12*(4), 259–263. https://doi.org/10.1038/s41561-019-0324-8

UNFCCC, C. (2015). *Adoption of the Paris agreement. I: Proposal by the president (draft decision)*. United Nations Office.

van Geldern, R., Schulte, P., Mader, M., Baier, A., & Barth, J. A. C. (2015). Spatial and temporal variations of pCO_2, dissolved inorganic carbon and stable isotopes along a temperate karstic watercourse. *Hydrological Processes*, *29*(15), 3423–3440. https://doi.org/10.1002/hyp.10457

Waldron, S., Scott, E. M., & Soulsby, C. (2007). Stable isotope analysis reveals lower-order river dissolved inorganic carbon pools are highly dynamic. *Environmental Science and Technology*, *41*(17), 6156–6162. https://doi.org/10.1021/es0706089

Wallin, M., Buffam, I., Öquist, M., Laudon, H., & Bishop, K. (2010). Temporal and spatial variability of dissolved inorganic carbon in a boreal stream network: Concentrations and downstream fluxes. *Journal of Geophysical Research*, *115*, 1–12. https://doi.org/10.1029/2009JG001100

Wallin, M. B., Grabs, T., Buffam, I., Laudon, H., Ågren, A., Öquist, M. G., & Bishop, K. (2013). Evasion of CO_2 from streams - the dominant component of the carbon export through the aquatic conduit in a boreal landscape. *Global Change Biology*, *19*(3), 785–797. https://doi.org/10.1111/gcb.12083

Wanninkhof, R. (1992). Relationship between wind speed and gas exchange over the ocean. *Journal of Geophysical Research*, *97*(C5), 7373–7382. https://doi.org/10.1029/92JC00188

Webb, J. R., Santos, I. R., Maher, D. T., & Finlay, K. (2019). The importance of aquatic carbon fluxes in net ecosystem carbon budgets: A catchment-scale review. *Ecosystems*, *22*(3), 508–527. https://doi.org/10.1007/s10021-018-0284-7

Weiss, R. F. (1974). Carbon dioxide in water and seawater: The solubility of a non-ideal gas. *Marine Chemistry*, *2*, 203–215. https://doi.org/10.1016/0304-4203(74)90015-2

Whitmore, K. M., Stewart, N., Encalada, A. C., Suárez, E., & Riveros-Iregui, D. A. (2021). Spatiotemporal variability of gas transfer velocity in a tropical high-elevation stream using two independent methods. *Ecosphere*, *12*(7). e03647. https://doi.org/10.1002/ecs2.3647

Zappa, C. J., McGillis, W. R., Raymond, P. A., Edson, J. B., Hintsa, E. J., Zemmelink, H. J., et al. (2007). Environmental turbulent mixing controls on air-water gas exchange in marine and aquatic systems. *Geophysical Research Letters*, *34*(10), 1–6. https://doi.org/10.1029/2006GL028790

Zolkos, S., Tank, S. E., Striegl, R. G., & Kokelj, S. V. (2019). Thermokarst effects on carbon dioxide and methane fluxes in streams on the peel plateau (NWT, Canada). *Journal of Geophysical Research: Biogeosciences*, *124*(7), 1781–1798. https://doi.org/10.1029/2019JG005038